nature medicine

ARTICLES

https://doi.org/10.1038/s41591-018-0128-1

Development of a gut microbe–targeted nonlethal therapeutic to inhibit thrombosis potential

Adam B. Roberts[1,2,9], Xiaodong Gu[1,2,9], Jennifer A. Buffa[1,2,9], Alex G. Hurd[1,2,7], Zeneng Wang[1,2], Weifei Zhu[1,2], Nilaksh Gupta[1,2], Sarah M. Skye[1,2], David B. Cody[3], Bruce S. Levison[1], William T. Barrington[4], Matthew W. Russell[1,2], Jodie M. Reed[3], Ashraf Duzan[2,5], Jennifer M. Lang[4], Xiaoming Fu[1,2], Lin Li[1,2], Alex J. Myers[1,8], Suguna Rachakonda[1,2], Joseph A. DiDonato[1,2], J. Mark Brown[1,2], Valentin Gogonea[1,2,5], Aldons J. Lusis[4], Jose Carlos Garcia-Garcia[3] and Stanley L. Hazen[1,2,6*]

Trimethylamine *N*-oxide (TMAO) is a gut microbiota–derived metabolite that enhances both platelet responsiveness and in vivo thrombosis potential in animal models, and TMAO plasma levels predict incident atherothrombotic event risks in human clinical studies. TMAO is formed by gut microbe–dependent metabolism of trimethylamine (TMA) moiety-containing nutrients, which are abundant in a Western diet. Here, using a mechanism-based inhibitor approach targeting a major microbial TMA-generating enzyme pair, CutC and CutD (CutC/D), we developed inhibitors that are potent, time-dependent, and irreversible and that do not affect commensal viability. In animal models, a single oral dose of a CutC/D inhibitor significantly reduced plasma TMAO levels for up to 3 d and rescued diet-induced enhanced platelet responsiveness and thrombus formation, without observable toxicity or increased bleeding risk. The inhibitor selectively accumulated within intestinal microbes to millimolar levels, a concentration over 1-million-fold higher than needed for a therapeutic effect. These studies reveal that mechanism-based inhibition of gut microbial TMA and TMAO production reduces thrombosis potential, a critical adverse complication in heart disease. They also offer a generalizable approach for the selective nonlethal targeting of gut microbial enzymes linked to host disease limiting systemic exposure of the inhibitor in the host.

Recent studies implicate participation of the gut microbiome in numerous facets of human health and disease[1–6]. For example, less than a decade ago, a link between dietary phosphatidylcholine, a nutrient common in a Western diet, gut microbiota–dependent generation of the metabolite TMAO, and cardiovascular disease (CVD) pathogenesis was first described[7]. Since then, multiple human and animal studies supporting both mechanistic and clinical prognostic associations between TMAO formation and cardiometabolic disease risks have been reported[8–16]. The mechanisms through which TMAO is thought to foster enhanced CVD risks are manifold and include alterations in tissue sterol metabolism[7,9,17], enhanced endothelial cell activation and vascular inflammation[7,18–20], and stimulation of profibrotic signaling pathways[14,15]. Historically, gut microbiota are known to impact factors linked to platelet function and hemostasis, including serotonin[21], vitamin K[22], and von Willebrand factor[23]. In addition, recent studies reveal TMAO alters calcium signaling in platelets, enhancing responsiveness and in vivo thrombosis potential in animal models[15]. Parallel clinical studies reveal TMAO levels are associated with thrombotic event risks (heart attack and stroke)[15], and clinical interventional studies with choline supplementation in healthy vegan or omnivorous volunteers were shown to both increase circulating TMAO levels and heighten platelet responsiveness to agonists[24]. Finally, several recent meta-analyses confirm a strong clinical association between increased levels of TMAO and incident adverse cardiovascular event and mortality risks in multiple populations[25–27]. Thus, there is rapidly growing interest in the therapeutic targeting of gut microbiota–dependent TMAO generation for the potential treatment of CVD[28].

TMAO is generated via a metaorganismal pathway that begins with gut microbial conversion of dietary nutrients (for example, phosphatidylcholine, choline, and carnitine) into TMA, followed by host liver oxidation to TMAO by flavin monooxygenases (FMOs)[29,30]. Given the abundance of the choline moiety in both bile[31] and common dietary staples (for example, eggs, meat and fish, and some fruits and vegetables), microbial conversion of choline into TMA likely accounts for a substantial portion of TMAO production in subjects, regardless of diet. A pair of microbial proteins encoded by genes of the choline utilization (*cut*) gene cluster, the catalytic CutC protein and its activating partner, CutD, support choline TMA lyase enzyme activity[32–34]. We recently reported the use of a natural product, 3,3-dimethyl-1-butanol (DMB), as a tool drug that inhibits microbial choline TMA lyase activity in vitro and in vivo[35]. When given to atherosclerosis-prone apolipoprotein E knockout (*ApoE*$^{-/-}$) mice on a choline-supplemented diet, plasma TMAO levels were significantly lowered, and concurrently, macrophage cholesterol accumulation, foam cell formation, and atherosclerotic lesion development were attenuated[35].

[1]Department of Cellular and Molecular Medicine, Lerner Research Institute, Cleveland Clinic, Cleveland, OH, USA. [2]Center for Microbiome & Human Health, Cleveland Clinic, Cleveland, OH, USA. [3]Life Sciences Transformative Platform Technologies, Procter & Gamble, Cincinnati, OH, USA. [4]Departments of Human Genetics and Medicine, David Geffen School of Medicine, University of California Los Angeles, Los Angeles, CA, USA. [5]Department of Chemistry, Cleveland State University, Cleveland, OH, USA. [6]Heart and Vascular Institute, Cleveland Clinic, Cleveland, OH, USA. [7]Present address: Department of Biostatistics, University of Pittsburgh, Pittsburgh, PA, USA. [8]Present address: Heritage College of Osteopathic Medicine, Ohio University, Athens, OH, USA. [9]These authors contributed equally: Adam B. Roberts, Xiaodong Gu, Jennifer A. Buffa. *e-mail: hazens@ccf.org

Although atherosclerotic plaque development is a defining pathologic feature of coronary artery disease, enhanced platelet reactivity and acute thrombotic occlusion of vessels are the proximate cause of myocardial infarction, stroke, and the majority of deaths in patients with CVD[36]. Use of antiplatelet agents has become a cornerstone for the treatment of CVD because of substantial reduction in CVD events and mortality[37,38]. However, more widespread use of antiplatelet agents has been limited by the increased risk of bleeding, which also leads to nonadherence[39–41]. Herein we show that a mechanism-based nonlethal inhibitor of the gut microbial TMAO pathway, designed to selectively accumulate within the gut microbial compartment, can serve as a new therapeutic approach for attenuating thrombosis while simultaneously limiting systemic exposure in the host.

Results

DMB attenuates choline diet–enhanced platelet responsiveness and in vivo rate of thrombus formation. In initial studies, C57BL/6 J mice were maintained on a chemically defined control 'chow' diet versus the same diet supplemented with choline (1% wt/wt). The choline diet elicited no differences in multiple indices of platelet activation, including surface phosphatidylserine content ($P=0.84$) in ADP-stimulated washed platelets or levels of von Willebrand factor ($P=0.14$), alpha granule release ($P=0.31$), or prothrombotic microvesicle release ($P=0.66$) in platelet-rich plasma (PRP) in the absence of agonist (Supplementary Fig. 1). However, as previously reported[15], choline supplementation resulted in tenfold-higher plasma TMAO levels ($P<0.0001$) and enhanced aggregometry response to submaximal levels of ADP (1 μM) in PRP ($P<0.0001$; Fig. 1a). Moreover, the TMAO-enhancing effect on stimulus-dependent platelet aggregation was also observed with washed platelets from mice fed the high-choline diet ($P=0.0002$) and was greatest at submaximal levels of agonist (ADP, collagen; Supplementary Fig. 1).

In parallel studies, mice were maintained on the chow versus choline-supplemented diet but also exposed to the tool drug DMB. DMB significantly reduced both TMAO levels ($P<0.0001$) and stimulus (ADP)-dependent platelet aggregation ($P=0.003$) in PRP recovered from choline-supplemented mice (Fig. 1a). In separate studies, DMB was directly incubated with the PRP preparations, and no effects on the platelet aggregometry responses, either with DMB alone or in the presence of agonist (ADP), were observed (Supplementary Fig. 2). Importantly, DMB-induced suppression of plasma TMAO levels and ADP-stimulated platelet aggregation responses in PRP recovered from choline-fed mice were completely reversed by direct injection of TMAO ($P=0.32$; Fig. 1a). Representative platelet aggregometry tracings for each group of mice are shown in Supplementary Fig. 3.

The carotid artery $FeCl_3$ injury model was next performed to quantify the rate of clot formation and time to vessel occlusion following injury in mice fed either chow or choline-supplemented diets with or without DMB (Fig. 1b,c). Choline supplementation resulted in marked TMAO elevation and shortening of vessel occlusion time ($P<0.0001$) as previously reported[15], and provision of DMB attenuated the choline diet–induced rise in TMAO and rate of clot formation ($P=0.002$; Fig. 1b,c). In separate studies, intraperitoneal injection of TMAO completely reversed DMB-dependent inhibition in choline diet–enhanced rate of thrombus formation (Fig. 1c). However, despite the high dose of DMB provided, choline diet–associated TMAO elevations, increased platelet aggregation, and shortened in vivo thrombus formation were not fully rescued compared to chow-fed mice (Fig. 1a,c). In light of these promising results, we sought to develop second-generation TMA lyase inhibitors with improved therapeutic potential.

Design and development of potent, mechanism-based, nonlethal microbial CutC/D inhibitors. We hypothesized that a suicide substrate mechanism-based inhibitor could possess many desirable advantages, including the selective targeting of a gut microbial pathway in a nonlethal manner, while potentially accumulating within the microbe thereby limiting systemic exposure of the drug in the host (i.e., as choline catabolism within the microbe was inhibited, cytosolic levels would increase, be sensed as an abundant nutrient, and trigger upregulation of the entire choline utilization gene cluster, including choline transporters). We therefore sought to develop an inhibitor that had the following characteristics: (i) it is a high affinity choline analog inhibitor; (ii) it is nonlethal to the microbe; (iii) it initially is inert (nonreactive); (iv) it can be transported into an intact gut microbe; and (v) it possesses a cryptic reactive moiety that is only revealed upon the unique cleavage of the C–N bond executed by microbial choline TMA lyase catalysis. This could in theory result in generation of a reactive species within the microbe that could then covalently modify an active site residue, promoting irreversible inhibition. With respect to these goals, we designed as a prototypic suicide substrate inhibitor the choline analog iodomethylcholine (IMC) (Fig. 1d). We predicted that after C–N bond cleavage by CutC, the product formed would be highly reactive and could lead to irreversible inactivation of the microbial enzyme, as quantum mechanical calculations using the CutC crystal structure derived from *Desulfovibrio alaskensis*[42] (see Methods) predict the rapid (concerted) loss of I^- and the potential for covalent attachment to nearby nucleophilic residues (Fig. 1d and Supplementary Fig. 4).

We developed a tiered screening assay system to test for broad efficacy among phylogenetically diverse commensal bacteria that contain CutC/D and robust choline TMA lyase activity. As previously reported[35], we used cloned *cutC* and *cutD* genes from *Proteus mirabilis* (ID: 6801039) and *D. alaskensis* (ID: 3926085) that were separately transformed into competent *Escherichia coli* cells. Choline TMA lyase activity was monitored in the clarified lysate using isotope-labeled choline (d_9[trimethyl]-choline) as the substrate and measuring the production of d_9-TMA. We also employed similar lysate and whole-cell culture assays using wild-type *P. mirabilis*, as well as stable polymicrobial human fecal cultures using a continuous flow bioreactor system (see Methods). Remarkably, IMC displayed an in vitro potency (IC_{50}) approximately 10,000 times greater than DMB against the recombinant *P. mirabilis* CutC/D lysate, recombinant *D. alaskensis* CutC/D lysate, and wild-type, whole-cell *P. mirabilis* in culture (Fig. 1e). In contrast to a recent report[43], resveratrol was largely ineffective in each of the screening assays employed (Fig. 1e) and showed no effect on plasma TMAO levels in vivo when administered to mice on a choline-supplemented diet ($P=0.91$; data not shown).

Having observed the potent inhibition in TMA production in vitro with IMC, we synthesized multiple alternative halomethylcholines, which as a group were remarkably effective in all lysate and whole-cell assays (Table 1 and Fig. 2a). Interestingly, the fluorinated choline analog, fluoromethylcholine (FMC), was the most potent halomethylcholine examined ($IC_{50}=900$ pM against *P. mirabilis* CutC/D), and in docking calculations, was predicted to have the tightest interaction with the active site of the CutC crystal structure derived from *D. alaskensis* (see Methods). FMC was also more potent than IMC against our polymicrobial, human fecal cultures ($EC_{50}=7.9$ nM and 1.6 μM, respectively; Table 1). In drug metabolism studies in mice, we detected low levels of halomethylbetaines (an oxidative metabolite) following oral halomethylcholine administration. We therefore synthesized each of the corresponding halomethylbetaines and screened them for inhibitory activity. In general, the halomethylbetaines were found to act as CutC/D TMA lyase inhibitors but were weaker than their choline counterparts by approximately 2–3 orders of magnitude (Table 1). Given the promising results observed with the halomethylcholines, both FMC and IMC were advanced for further mechanistic and preclinical studies.

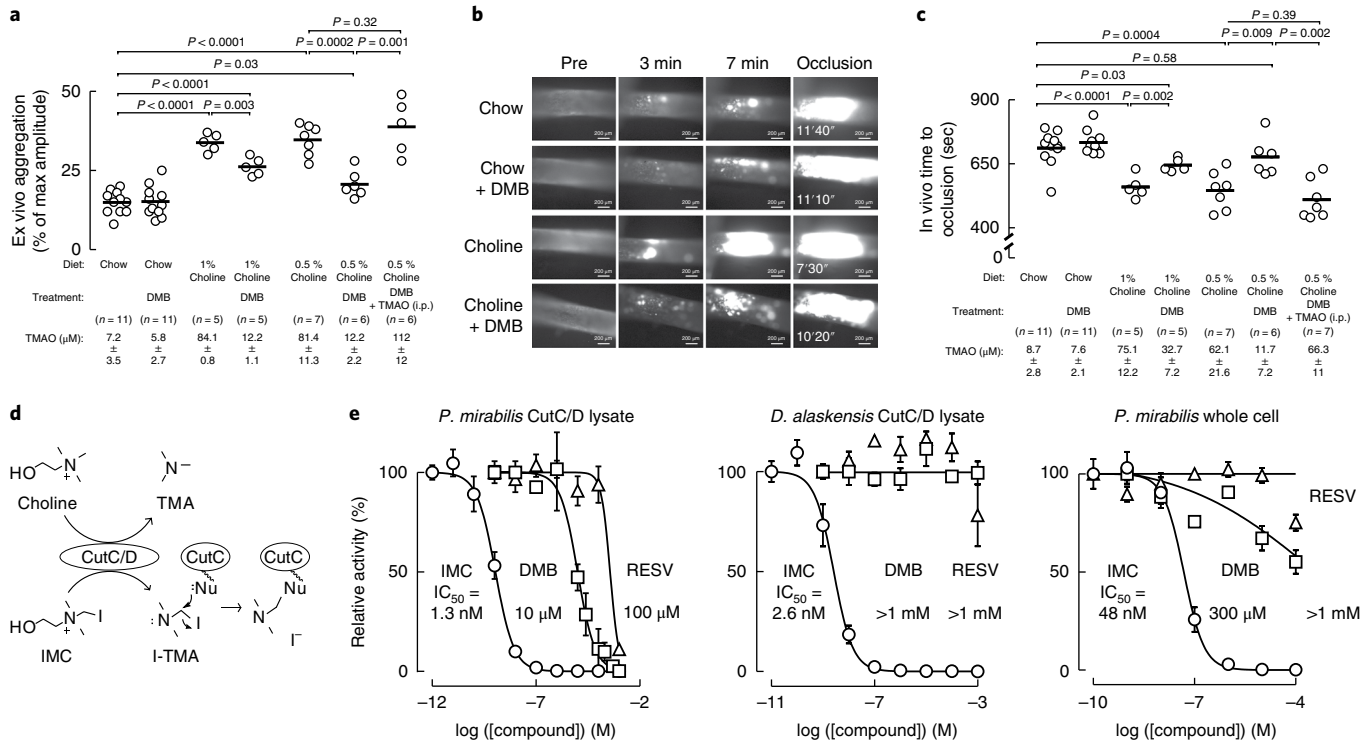

Fig. 1 | Proof of concept that microbial choline TMA lyase inhibition can attenuate choline diet–enhanced platelet aggregation and in vivo thrombus formation. a, Platelet aggregation in PRP of mice fed the indicated diets ± DMB (1.3% vol/vol) provided in drinking water for 6 weeks. Platelet aggregation was measured in response to a submaximal concentration of ADP (1 μM). Data points represent aggregation as the percentage of maximum amplitude in PRP recovered from each mouse, and bars represent mean levels for each group. Plasma TMAO levels are also shown and represent mean ± s.e.m. for each group. Significance was determined by two-tailed Student's *t*-test. **b**, Representative vital microscopy images of carotid artery thrombus formation at the indicated time points following $FeCl_3$-induced carotid artery injury in mice fed either a chemically defined chow or 1% choline diet with or without the addition of DMB (1.3% vol/vol). The time to complete occlusion is noted in the right-hand panels. Complete study results including replications are shown in Fig. 1c. **c**, Quantification of in vivo thrombus formation following $FeCl_3$-induced carotid artery injury in mice fed the indicated diets with or without DMB (1.3% vol/vol) provided in drinking water for 6 weeks. Data points represent the time to cessation of flow for each mouse, and bars represent mean levels for each group. Plasma TMAO levels are also shown and represent mean ± s.e.m. for each group. Significance was determined by two-tailed Student's *t*-test. **d**, Proposed mechanism by which a potential suicide substrate inhibitor of CutC/D, IMC, can form a reactive iodotrimethylamine (I-TMA) product that can promote irreversible CutC/D inhibition via covalent modification of a reactive, nucleophilic active-site residue (Nu). **e**, Comparison of the inhibitory potency of IMC (○), DMB (□), and resveratrol (RESV, Δ) against wild-type, recombinant *P. mirabilis* CutC/D lysate (left), recombinant *D. alaskensis* CutC/D lysate (center), and whole-cell (intact live culture) wild-type *P. mirabilis* (right). Data points represent the mean ± s.e.m. Exact numbers used for each data point can be found in the Source Data ($n = 2$–9 technical replicates).

To better understand the mechanism of inhibition, we first characterized the kinetics of IMC- and FMC-dependent inhibition of recombinant CutC/D, as time-dependent enhancement in enzyme inactivation is a characteristic feature of suicide substrate inhibitors[44,45]. As expected, both IMC and FMC demonstrated enhanced inhibitory potency following longer times of preincubation with the enzyme before the addition of d_9-choline substrate (Fig. 2b). Second, as anticipated for a mechanism-based mode of inhibition, the inactivation of CutC/D by both IMC and FMC were irreversible, as dialysis failed to rescue enzyme activity. In contrast, reversible inhibition of CutC/D activity following dialysis was observed with an alternative, potent inhibitor that we developed called phenylcholine ($IC_{50} = 150$ nM against *P. mirabilis* CutC/D) (Fig. 2c).

We further examined the behavior of FMC and IMC interaction with recombinant *P. mirabilis* CutC/D using Michaelis–Menten kinetics. Addition of FMC at increasing concentrations lowered maximal enzyme velocity (V_{max}) with no apparent effect on substrate affinity (K_M) (Supplementary Fig. 5), indicating that FMC acts kinetically as a noncompetitive inhibitor. Increasing concentrations of IMC similarly decreased V_{max}, but also increased K_M (Supplementary Fig. 5), indicating that IMC acts kinetically as a mixed mechanism inhibitor, with elements of both competitive and noncompetitive inhibition. In an effort to demonstrate an enzyme-inhibitor adduct, we performed multiple mass spectrometry studies but were unable to find a covalent adduct between IMC or FMC with either CutC or CutD. Nevertheless, both IMC and FMC display numerous characteristics consistent with a covalent mode of inhibition (time-dependent, irreversible, and noncompetitive inhibition), which is also consistent with our initial hypothesized, quantum-mechanical-derived reaction mechanism based on a suicide substrate (Fig. 1d and Supplementary Fig. 4).

Importantly, both IMC and FMC were nonlethal, even at high concentrations (1 mM). Moreover, neither affected the growth rate of several known TMA-producing human commensals (*P. mirabilis*, *Escherichia fergusonii*, and *Proteus penneri*)[33,46] when cultured in nutrient-rich medium under conditions showing complete inhibition in choline TMA lyase activity (Fig. 2d). In studies with prolonged exposures to either IMC or FMC, no reductions in apparent microbial fitness (growth rate or density) were observed (Supplementary Fig. 6).

FMC and IMC sustainably suppress host TMAO levels without observed toxicity. In initial experiments, mice were placed on a choline-supplemented diet, and subsequent provision of either

Table 1 | Summary of the inhibitory potency across multiple screens of halomethylcholine and halomethylbetaine analogs

Name	In vitro clarified lysate IC_{50} (nM)			Whole-cell EC_{50} (nM)	Ex vivo EC_{50} (nM)	In vivo EC_{50} (mg/kg/day)	
	rec. CutC/D *P. mirabilis*	rec. CutC/D *D. alaskensis*	Wild-type *P. mirabilis*	Wild-type *P. mirabilis*	Fecal polymicrobial	q24h postgavage	d_9-choline challenge
Fluoromethylcholine (FMC)	0.9	1.4	2.0	56	7.9	3.4	0.01
Iodomethylcholine (IMC)	1.3	2.6	1.5	48	1,600	45	0.2
Chloromethylcholine (CMC)	3.0	2.8	8.9	45	63	15.3	0.02
Bromomethylcholine (BMC)	7.8	5.6	4.4	40	160	>310	0.03
Iodomethylbetaine (IMB)	400	350	2,600	14,000	250,000	>310	19.3
Bromomethylbetaine (BMB)	2,800	3,100	1,300	9,400	130,000	>310	9.5
Fluoromethylbetaine (FMB)	9,100	14,000	16,000	320,000	79,000	300	58.9
Chloromethylbetaine (CMB)	9,800	11,000	5,000	81,000	50,000	>310	83.3

Numbers shown represent either IC_{50} or EC_{50} values for the indicated halomethylcholine or halomethylbetaine compound, as tested in the indicated in vitro enzyme activity screen, in vitro culture of intact individual (*P. mirabilis*) or polymicrobial (human fecal) culture, or one of two different in vivo screening strategies. For all in vitro or ex vivo studies, calculated IC_{50} or EC_{50} values represent results from dose–response curves with between 6 and 11 different concentrations monitored. Exact numbers used for each data point can be found in the Source Data. For the in vivo studies, calculated EC_{50} doses use data either from (i) the d_9-choline challenge model, which gives an estimate of the oral dose needed to inhibit 50% of microbial d_9-choline → d_9-TMAO in mice, or (ii) the q24h postgavage model, which gives an estimate of the oral dose needed to inhibit 50% of plasma level of TMAO at trough time in a chronic, once daily oral gavage dosing regimen in mice maintained on a high choline (1% wt/wt) diet. In vivo dose–response curves employed at least 4 or 5 animals per dose examined, with 6–10 different inhibitor concentrations examined for each compound. See Source Data for exact sample numbers for each experiment performed and each independent experimental dose–response curve included in the cumulative analysis used to calculate IC_{50} or EC_{50} values in each cell.

IMC or FMC as a single oral dose via gastric gavage resulted in marked inhibition of plasma TMAO levels (>95% inhibition, $P<0.0001$; Fig. 3a). We next progressed to a chronic daily exposure study, treating mice on a choline-supplemented diet with inhibitor via oral gavage once a day for 2 weeks, monitoring plasma TMAO at time of trough (24 h postgavage), resulting in virtually complete inhibition in circulating TMAO levels (Fig. 3a and Supplementary Fig. 7). In dose–response studies, both FMC and IMC showed dose-dependent suppression in both TMA production ($EC_{50}=4.5$ and 31 mg per kg body weight (mg/kg), respectively; Supplementary Fig. 8) and systemic TMAO levels, with FMC demonstrating potency greater than IMC by an order of magnitude ($EC_{50}=3.4$ and 45 mg/kg, respectively; Fig. 3a and Table 1). We also examined the in vivo dose–response curves for microbial choline TMA lyase inhibition by quantifying d_9-TMA and d_9-TMAO production from d_9-choline provided concomitantly with the inhibitor as a single oral gavage. Under these conditions, both FMC and IMC demonstrated remarkable capacity to suppress production of d_9-TMA ($EC_{50}=0.008$ and 0.5 mg/kg, respectively; Supplementary Fig. 8) and d_9-TMAO ($EC_{50}=0.01$ mg/kg and 0.2 mg/kg, respectively; Table 1 and Fig. 3a).

We next examined both the pharmacokinetics and functional metabolic effects of oral FMC and IMC provision by measuring plasma, fecal, and urinary levels of the drugs, their metabolites, and both choline and its microbial- and host-derived metabolites over time in mice fed a high-choline diet. Results with FMC (Fig. 3 and Supplementary Fig. 9) and IMC (Supplementary Fig. 10) were similar, with FMC showing enhanced potency and sustained duration of inhibition. FMC and IMC were detectable at low (μM) levels only for the first few hours in plasma, but their halomethylbetaine oxidation products, fluoromethylbetaine (FMB) and iodomethylbetaine (IMB), were ~10-fold more abundant, reaching their peak level 2 h postgavage (Fig. 3b and Supplementary Fig. 10). Despite intensive screening at multiple time points, other potential metabolites, including the halide-substituted versions of TMA and the predicted intermediate trimethylhalide-imines (Supplementary Fig. 4), were not detected in plasma, urine, or fecal samples. Importantly, analyses of feces revealed that the majority of FMC and IMC remains in the gut luminal compartment, with only nominal levels of FMB or IMB present in fecal samples (Fig. 3b and Supplementary Fig. 10). Modest but relatively equal amounts of FMC and FMB (Supplementary Fig. 9) and IMC and IMB (Supplementary Fig. 10) were observed in urine.

Both FMC and IMC induced an almost complete reduction in plasma TMA and TMAO levels following a single oral dose (via gavage) for a sustained period, with FMC demonstrating a striking trough that persisted for over 3 d (Fig. 3b) and IMC for over 2 d postgavage (Supplementary Fig. 10). For TMA and TMAO, these same trends were observed in urine and feces following administration of either FMC or IMC (Supplementary Figs. 9 and 10). After gavage of either FMC (Fig. 3b) or IMC (Supplementary Fig. 10), plasma betaine levels were modestly increased before returning to baseline. Choline (via betaine) can enter into metabolic pathways related to one-carbon methyl donors; however, following single or chronic dosing with FMC or IMC, no changes were noted in plasma levels for homocysteine, dimethylglycine, or folate pathway–related metabolites (all $P>0.05$, data not shown). Analyses of fecal samples revealed significant increases in choline levels following FMC or IMC administration, which were extremely low before addition of the inhibitor (Supplementary Figs. 9 and 10). Importantly, no significant effects on plasma choline levels were observed (Fig. 3b and Supplementary Fig. 10). These results are interesting in light of recent reports by Rey and colleagues[33,47] suggesting that gut microbiota, via the CutC/D pathway, may play a significant role in choline bioavailability in the host.

No signs of toxicity were observed in mice following chronic exposure to wholly effective doses of FMC (10 mg/kg) or IMC (100 mg/kg) (Supplementary Fig. 11). This included no indications

of body weight loss, grooming or other behavioral problems, or adverse effects on renal functional measures (serum creatinine, blood urea nitrogen (BUN)), liver function tests (alanine transaminase (ALT), aspartate transaminase (AST), BUN), and hematology-related measures (hemoglobin, hematocrit, and complete blood cell count (CBC) with differential that remained within the normal range)[48]. In addition, plasma levels of choline and betaine were not significantly different (from vehicle) with chronic exposure to either FMC or IMC, and neither FMB nor IMB showed evidence of accumulation in plasma (Supplementary Fig. 12). In alternative studies in both male and female mice with more prolonged exposures (15–20 weeks) to IMC, no adverse effects were observed, including normal indices of renal function, liver function, and CBC with differential (data not shown). Screening of IMC and FMC in a battery of pharmacological safety tests failed to show: (i) inhibition in human ether-a-go-go-related gene (hERG) channel function; (ii) toxicity to mitochondria in HepG2 cells cultured in glucose- or galactose-supplemented medium; (iii) adverse effects on the viability of HK-2 cells in culture; or (iv) adverse signals during AMES testing at levels up to 1,000 μg per well (Supplementary Table 1).

IMC and FMC are preferentially sequestered within gut microbes. As part of our drug development design, we hypothesized that sustained inhibitory activity could be achieved following single-dose exposures if the inhibitors were nonlethal and selectively accumulated within the microbe by induction of the *cut* gene cluster, which contains an active choline transporter. In other words, with active transport of the inhibitor into the microbe and accumulation to high levels, it would take multiple bacterial divisions to slowly and progressively deplete microbe intracellular inhibitor concentration until it was below the therapeutic threshold before TMA production from choline would occur. To test for this, we performed experiments in which gut microbes were recovered from different segments of the intestines 4 h after a single oral gavage with either FMC, IMC, or vehicle in mice fed a high-choline diet. Strikingly, within the large intestine (cecum and colon), the anatomic location where the majority of choline TMA lyase–harboring commensals reside[49], we observed the selective accumulation of each inhibitor to the millimolar level (2–6 mM), virtually complete elimination in detectable luminal TMA (product), and a similar marked increase in intestinal microbial choline (substrate) levels (Fig. 3c). Levels of halomethylbetaines in all intestinal segments were substantially lower than their halomethylcholine counterparts, and there were no statistically significant effects on gut luminal betaine or TMAO levels (Supplementary Fig. 13).

Microbial TMA lyase inhibition suppresses diet-induced platelet phenotypes. In further studies, mice were placed on either chow or choline-supplemented diets in the absence or presence of inhibitors to determine the effects of the inhibitors on choline diet–enhanced platelet aggregation. Results confirmed complete suppression of choline diet–enhanced TMAO generation and accompanying enhancement in ADP-dependent platelet aggregation response with provision of either FMC ($P=0.0001$) or IMC ($P=0.001$; Fig. 4a). Representative platelet aggregometry tracings from each group are shown in Supplementary Fig. 3. Furthermore, provision of IMC to the mice was shown to reverse choline diet–induced effects on not only multiple indices of platelet responsiveness using distinct agonists (for example, ADP, collagen) in PRP, but also in ADP-stimulated isolated platelets (Supplementary Fig. 14). In additional control studies, FMC and IMC were directly incubated with PRP from both mice and humans (with or without agonist), and no effects on platelet aggregometry responses were observed. Their primary in vivo metabolites, FMB and IMB, also did not affect platelet aggregometry responses in human PRP (Supplementary Fig. 2). We next examined the effect of IMC on choline diet–dependent enhancement in platelet adhesion within whole blood using a microfluidic device under conditions of physiological levels of shear stress. Provision of IMC reversed choline diet–dependent increases in both TMAO levels and platelet adherence to collagen matrix to levels observed in chow-fed mice (Fig. 4b).

The impact of FMC and IMC on in vivo thrombus formation was next examined using the carotid artery $FeCl_3$-induced injury model. When mice were placed on either chow or choline-supplemented diets, in the absence or presence of inhibitor (0.06% IMC or 0.006% FMC), provision of either FMC ($P<0.0001$) or IMC ($P<0.0001$) completely blocked choline-supplemented diet–induced increases in both plasma TMAO and in vivo rate of clot formation (Fig. 4c,d). Importantly, neither FMC ($P=0.85$) nor IMC ($P=0.73$) led to a prolongation in occlusion time beyond that observed with normal chow. In these animals, we also investigated potential effects of FMC and IMC on the regulation of the microbial *cut* gene cluster within the cecal polymicrobial community. As a prototypic gene within the cluster, we quantified *cutC* expression via recovered cecal microbial RNA by qPCR. Notably, global cecal microbial *cutC* expression was significantly upregulated by the addition of either FMC or IMC in chow diet in the absence of added choline (Fig. 4e). Similar enhanced *cutC* expression was also seen in mice that received choline supplementation relative to those fed chow. Addition of FMC or IMC to the choline-supplemented diet groups failed to further increase microbial expression of *cutC* (Fig. 4e).

In further studies, we examined the impact of FMC and IMC on in vivo bleeding time. Mice were again placed on either chow or choline-supplemented diets with or without FMC or IMC, and then bleeding time was determined using a tail-tip amputation model[50]. Although TMAO levels were markedly suppressed, neither FMC nor IMC induced a significant change in bleeding potential, as monitored by multiple different measures including cumulative bleeding time ($P=0.90$) (Fig. 4f), hemoglobin loss ($P=0.14$), and weight loss from bleeding ($P=0.51$) (Supplementary Fig. 15).

Inhibition of microbial choline TMA lyase activity shifts intestinal microbial communities. While the halomethylcholines developed are nonlethal to cultured microbes when alternative nutrients are available (Fig. 2d), we sought to determine whether they induce a shift in gut microbial composition in vivo. Cecal microbial DNA encoding 16 S ribosomal RNA was sequenced from mice to examine the impact of IMC on in vivo thrombus formation (a subset of mice in Fig. 4d). Principal coordinates analysis (PCA) of microbial taxa revealed distinct clusters, indicating that both dietary choline supplementation and IMC exposure each induced significant ($P=0.001$) rearrangements in microbial composition (Fig. 5a). Performance of linear discriminant analysis coupled with effect size measurements permitted further identification of microbial taxa whose proportions accounted for significant characteristic differences observed in the chow versus choline-supplemented diets, as well as IMC-treated versus non-IMC-treated groups (Fig. 5b and Supplementary Fig. 16).

We also examined whether the proportions of any of the detected cecal genera within all groups of mice were significantly correlated with both plasma TMAO levels and in vivo thrombosis potential as quantified by time to carotid artery vessel occlusion during the $FeCl_3$-induced injury model. Provision of a high-choline diet was associated with both significant increases (for example, *Dehalobacterium* and *Adlercreutzia*) and reductions (for example, *Bifidobacterium*) in the proportions of several genera, which were each also significantly associated with both TMAO levels and time to vessel occlusion; moreover, these shifts in proportions were reversed with the addition of IMC ($P<0.0001$; Supplementary Fig. 17). In parallel studies, the impact of FMC treatment on choline

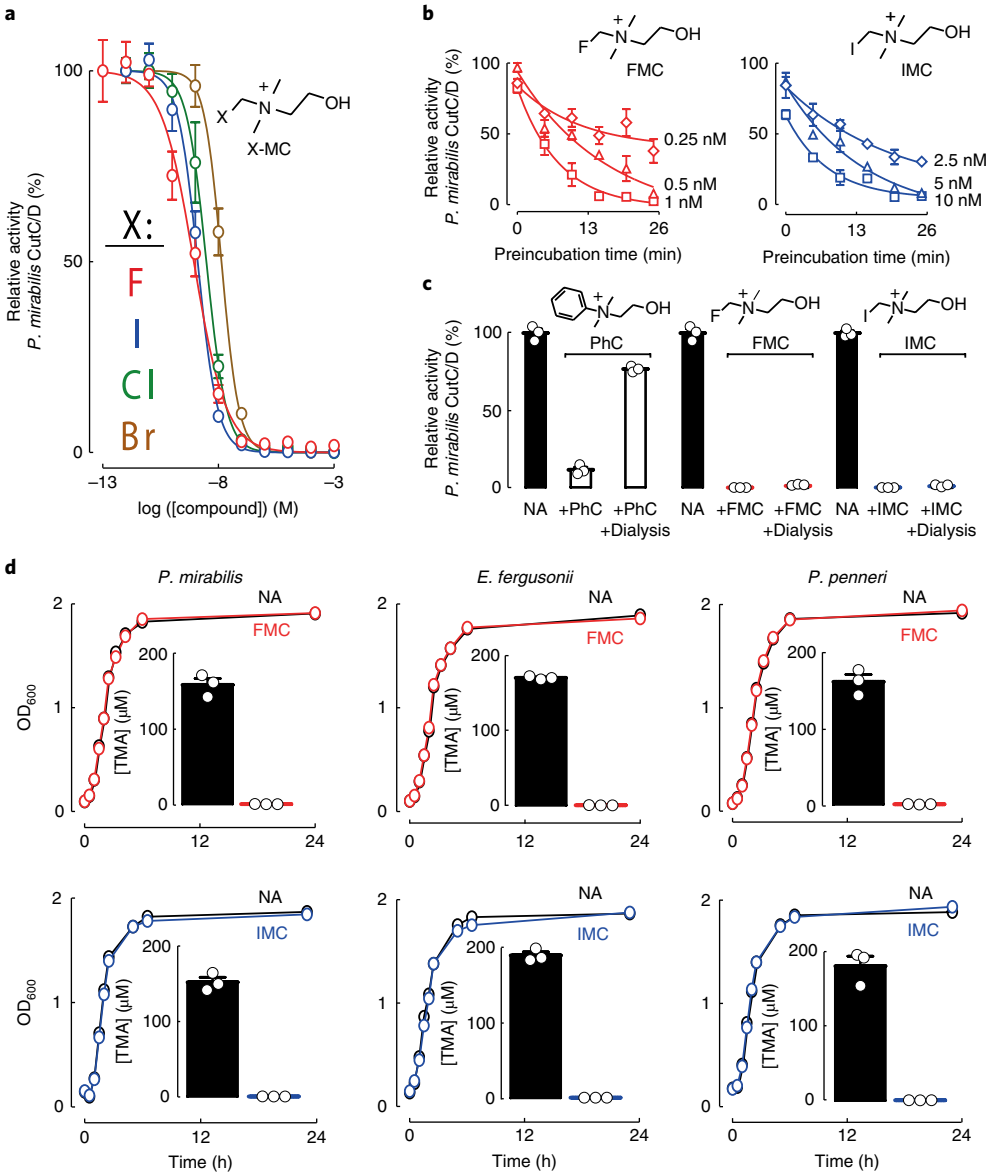

Fig. 2 | IMC and FMC are nonlethal, irreversible, and noncompetitive CutC/D inhibitors. a, Dose–response curves for halide-substituted (fluorine, F; iodine, I; chlorine, Cl; bromine, Br) methyl-choline analogs (X-MC) against recombinant *P. mirabilis* CutC/D lysate. Data points represent mean ± s.e.m. Exact numbers used for each data point can be found in the Source Data ($n = 3$–9 technical replicates). **b**, The time-dependence of the inhibitory potency as assessed by preincubating the indicated concentrations of FMC or IMC with recombinant *P. mirabilis* CutC/D lysate for increasing intervals before the addition of d_9-choline substrate and subsequent quantification of choline TMA lyase activity. Relative activity was measured against no inhibitor controls during the initial kinetic phase. Data points represent the mean ± s.e.m. Exact numbers used for each data point can be found in the Source Data ($n = 2$–9 technical replicates). **c**, Characterization of the reversibility of FMC, IMC, and phenylcholine (PhC) inhibition of recombinant *P. mirabilis* CutC/D lysate. Data points represent the mean ± s.e.m. ($n = 3$ technical replicates for each). NA, vehicle treatment. **d**, Growth of the indicated human TMA-producing gut commensals after culture with or without FMC (top) or IMC (bottom) in nutrient-rich broth. Inset bar graphs show TMA lyase activity calculated during the log-phase of growth ($OD_{600} = 0.5$). Growth curves shown are from representative experiments ($n = 3$ technical replicates), and TMA quantification represents the mean ± s.e.m.

diet–induced changes in cecal microbial composition showed analogous results (Supplementary Fig. 18). Interestingly, both IMC and FMC treatment in choline-supplemented mice induced a significant increase in the proportions of *Akkermansia* (Supplementary Figs. 17 and 18), a genus of considerable interest because of its reported links to improvement in obesity and metabolic health[51].

Discussion

The growing recognition of a contributory role of gut microbiota to both health and disease susceptibility promises that efforts to 'drug the microbiome', which are still in their infancy, may someday become commonplace in medicine. Herein we describe the development and characterization of potent inhibitors of gut microbiota–dependent TMA and TMAO generation that might serve as therapeutic agents capable of reducing thrombosis risk (Fig. 5c). In contrast to current antiplatelet drugs, which target mammalian enzymes (for example, COX1) or receptors (for example, $P2Y_{12}$ and PAR1)[52] and are limited in use by their potential for untoward bleeding, inhibition in microbial TMAO generation would not hypothetically suppress platelet function 'below normal' and thus

heighten bleeding risks. Further, given the unorthodox characteristics of a gut microbial pharmacological target, one can envision developing drugs that optimally target a gut microbial pathway mechanistically linked to disease susceptibility while limiting systemic exposure in the host.

One potential theoretical difficulty in 'drugging the microbiome' is that if every related microbial enzyme with similar function is not inhibited, there exists potential for compensation from alternative species, possibly limiting overall change in total microbial community activity. To overcome this issue, our drug development program incorporated several features. First, recognizing that microbial catabolic enzyme systems, such as the *cut* cluster, typically contain coordinately regulated genes, including a microbial transporter that actively transports the substrate into the microbe[53,54] to enable rapid exploitation of increased availability of an abundant nutrient[55], we speculated that development of a substrate analog inhibitor that irreversibly inactivated its target while retaining the ability to be used by the microbial transporters could produce a rise in microbial cytosolic substrate concentration. This might produce a 'feed-forward' cycle whereby both the substrate and the drug (substrate analog) are actively transported and sequestered within the microbe in proportion to the extent of inhibition. Indeed, we saw that by blocking choline catabolism with the potent CutC/D inhibitors, *cutC* expression is significantly increased in cecal microbes without dietary choline supplementation. And both choline and the inhibitors reached remarkably high gut microbial intracellular levels in the cecum and colon. Thus, our system of inhibition appears to create a positive feedback loop whereby the microbes in which the halomethylcholines potently block choline catabolism are transformed into virtual 'vacuum sweepers' for both choline and inhibitor accumulation. Microbes in the immediate environment that are not as potently inhibited directly might still thus have reduced TMA generation as they become starved of extracellular choline substrate.

Our efforts to develop inhibitors were also helped by the fact that there are no known mammalian enzymes that can cleave the C–N bond of choline[54]. We therefore sought to develop selective, nonreactive choline analogs that contain a cryptic reactive group that might become liberated upon enzymatic cleavage by the unique microbial enzymes (i.e., suicide substrate mechanism-based inhibitors) that produce TMA, the precursor for TMAO generation. We also used a comprehensive screening strategy that included phylogenetically diverse recombinant microbial choline TMA lyase enzymes and both mono- and polymicrobial (human fecal) assays to ensure the broad efficacy needed to inhibit a range of microbial choline TMA lyase enzymes from diverse taxa while also increasing the chances for development of highly potent inhibitors in vivo. Although we designed IMC to be the prototypical mechanism-based inhibitor, FMC proved to be more potent. Indeed, fluorine substitution can confer properties beneficial to the chemistry of suicide substrate inhibitors and their potential use as pharmaceuticals[56].

Kinetic analyses demonstrate that IMC and FMC are noncompetitive, time-dependent, and irreversible, which are hallmarks of mechanism-based inhibitors. However, despite extensive efforts, we were not able to find a covalent inhibitor–enzyme adduct via mass spectrometry. Upon observing that IMC shows kinetic evidence of both competitive and noncompetitive forms of inhibition, we hypothesize that there exist several potential avenues for halomethylcholines to serve as suicide substrate inhibitors and promote irreversible, covalent attachment to multiple nucleophilic amino acid targets (Supplementary Fig. 4). This potential along with their high inhibitory potency make detection more elusive. Nonetheless, both FMC and IMC proved nonlethal to human commensals when cultured in nutrient-rich broth under conditions demonstrating full inhibition of microbial choline TMA lyase activity. In mice, FMC and IMC lowered plasma TMAO levels over a prolonged period with limited systemic exposure. Moreover, by inhibiting gut microbial choline

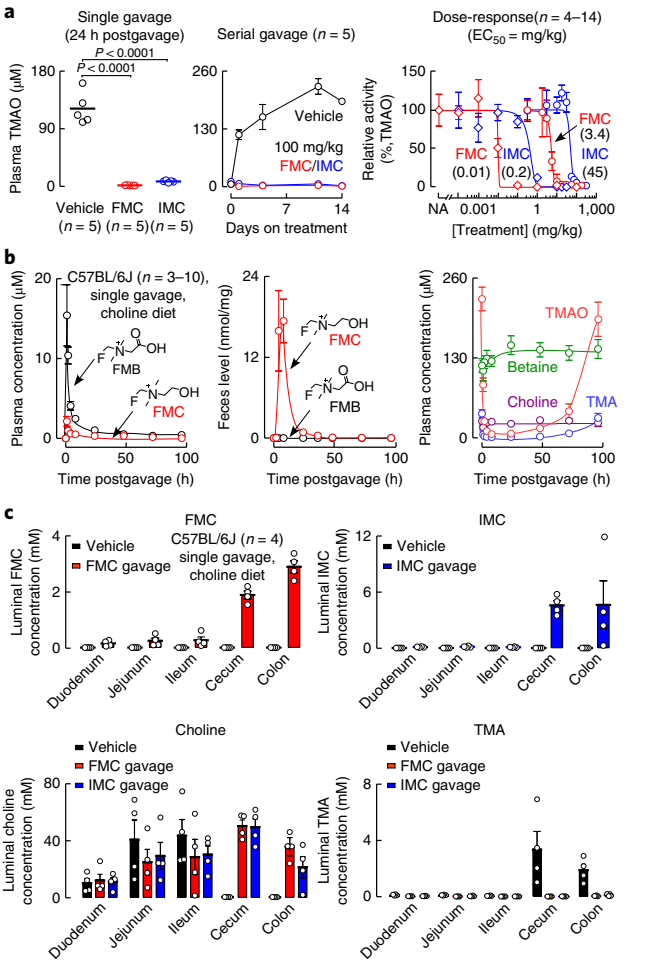

Fig. 3 | The in vivo pharmacokinetic and pharmacodynamic properties of FMC and IMC. a, Left, Plasma TMAO levels 24 h postgavage of vehicle, 100 mg/kg FMC, or 100 mg/kg IMC in mice maintained on a choline-supplemented (1% wt/wt) diet. Significance was determined by two-tailed Student's *t*-test. Center, Plasma TMAO levels (determined at 24 h postgavage) on the indicated days over a course of daily FMC or IMC treatment for 14 d. Right, Relative activity (compared to vehicle controls) in mice treated by oral gavage with either vehicle (NA) or the indicated range of doses (0.0001–310 mg/kg) of either FMC or IMC. For each inhibitor, two groups of mice were tested. In the 'd_9-choline challenge' group (◊), in which mice were maintained on a chemically defined chow diet (0.08% wt/wt total choline) and simultaneously gavaged with 10 mg/mL d_9-choline plus the indicated dose of FMC or IMC, the relative activity was measured in blood collected 3 h post-gavage as the amount of d_9-TMAO produced relative to the vehicle control (100%). In the 'q24h postgavage' group (O), mice were maintained on a choline-supplemented diet (1% wt/wt) and treated with once daily oral gavages of the indicated inhibitor and dose for 4 d; the relative activity represents plasma TMAO levels relative to the vehicle control in blood collected 24 h after the last gavage (on day 5). Data points represent the mean ± s.e.m. Exact numbers of mice used for each data point can be found in the Source Data (n = 4–14). **b**, Plasma levels of FMC and FMB (left) and choline, betaine, TMA, and TMAO (right) at the indicated time points after a single oral gavage of FMC (100 mg/kg) in mice maintained on a choline-supplemented diet (1% wt/wt) for 3 weeks. Center, levels of FMC and FMB in fresh fecal samples, normalized to the dry weight of the samples. Data points represent the mean ± s.e.m. Exact numbers of mice used for each data point can be found in the Source Data (n = 3–10). **c**, Concentrations of FMC, IMC, choline, and TMA within the indicated intestinal luminal compartment 4 h after a single gavage of either vehicle, 100 mg/kg FMC, or 100 mg/kg IMC in mice maintained on a choline-supplemented diet (1% wt/wt) for 3 weeks. Bars represent the mean ± s.e.m. for the indicated number of mice.

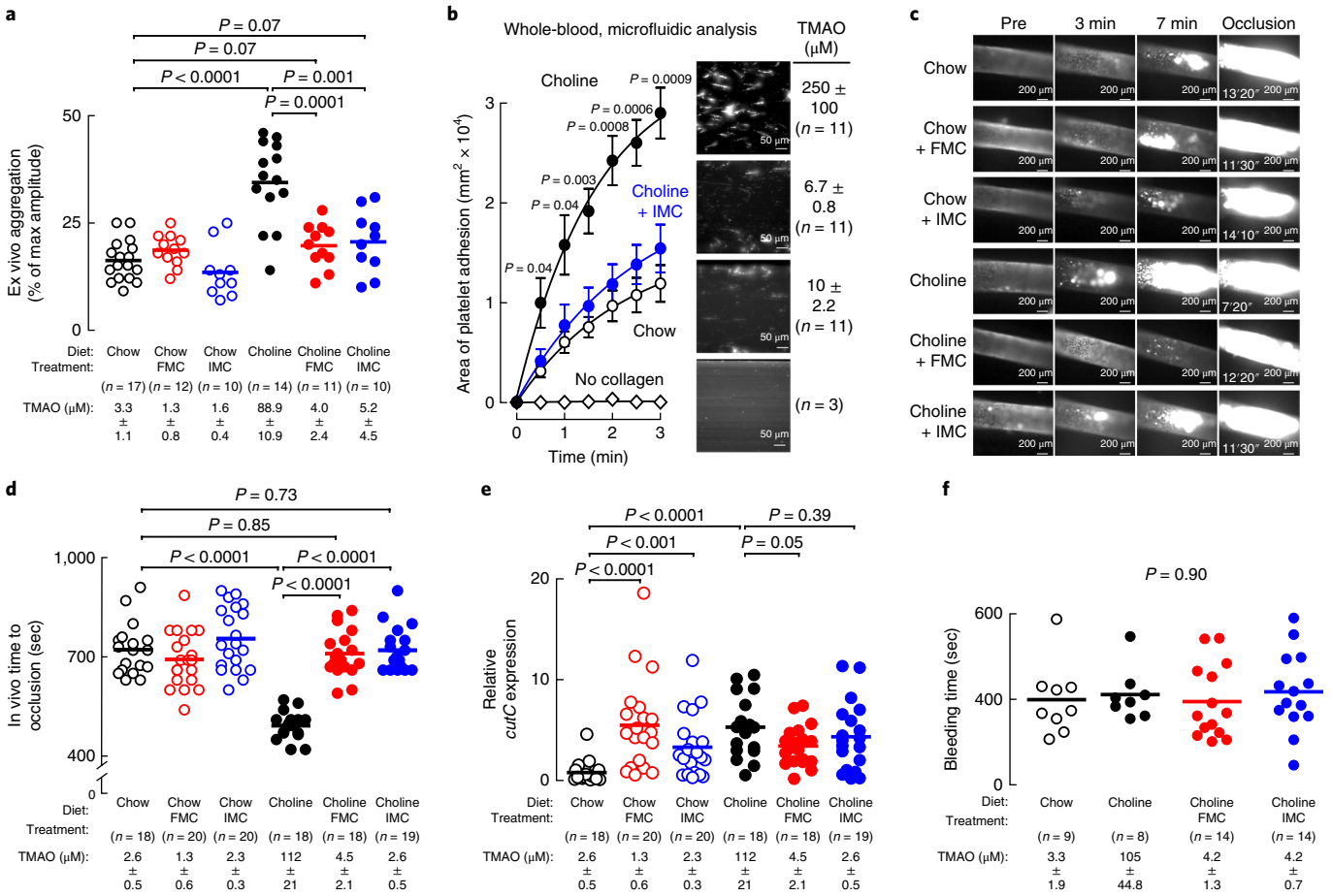

Fig. 4 | The mechanism-based CutC/D inhibitors IMC and FMC reverse choline diet–enhanced platelet responsiveness and thrombus formation. **a**, Platelet aggregation in PRP of mice fed the indicated diets with or without FMC (0.006% wt/wt) or IMC (0.06% wt/wt) for 2 weeks. Platelet aggregation was measured in response to a submaximal concentration of ADP (1 μM). Data points represent aggregation as the percentage of maximum amplitude in PRP recovered from each mouse, and bars represent mean levels for each group. Plasma TMAO levels are also shown and represent mean ± s.e.m. for the indicated number of mice for each group. Significance was determined by two-tailed Student's *t*-test. **b**, Adherence of fluorescently labeled platelets in whole-blood samples to a collagen-coated microfluidic biochip under physiological shear stress from mice fed the indicated diets (0.06% wt/wt IMC) for 2 weeks. Images show fluorescently labeled platelets adhered to the collagen-coated microchannel representative for each treatment group at the endpoint (3 min). Data points represent the mean ± s.e.m. for the indicated numbers of mice. Plasma TMAO levels are also shown and represent mean ± s.e.m. for each group. Significance between 'Choline' and 'Choline + IMC' groups was determined by two-tailed Student's *t*-test. **c**, Representative vital microscopy images of carotid artery thrombus formation at the indicated time points following $FeCl_3$-induced carotid artery injury in mice fed the indicated diets for 2 weeks. The time to complete vessel occlusion is noted in the right-hand panels. Cumulative study results for the indicated number of mice in each group are shown in Fig. 4d. **d**, Quantification of in vivo thrombus formation following $FeCl_3$-induced carotid artery injury in mice fed the indicated diets with or without FMC (0.006% wt/wt) or IMC (0.06% wt/wt) for 2 weeks. Data points represent the time to cessation of flow for each mouse, and bars represent mean levels for each group. Plasma TMAO levels are also shown and represent mean ± s.e.m. for each group. Significance was determined by two-tailed Student's *t*-test. **e**, Relative expression of microbial *cutC* in the cecal contents of the mice used in Fig. 4d, as determined by qPCR. Data points represent relative *cutC* expression for each mouse, and bars represent mean levels for each group. Significance was determined by two-tailed Student's *t*-test. **f**, Bleeding time following tail-tip amputation in the indicated number of mice fed the indicated diets (0.006% wt/wt FMC; 0.06% wt/wt IMC) for 1 week. Data points represent the cumulative bleeding time over 10 min for each mouse, and bars represent mean levels for each group. Plasma TMAO levels are also shown and represent mean ± s.e.m. for each group. Significance was determined using one-way ANOVA.

consumption, fecal choline content substantially increased without impacting plasma choline levels. These results suggest that inhibition in microbial choline utilization will not only suppress TMA and TMAO generation, but also may help enhance choline bioavailability for the host.

It is also notable that both IMC and FMC induced a shift in mouse cecal microbiota composition, particularly on a choline-supplemented diet, reversing choline-induced changes in the proportions of certain taxa. Thus, eliminating selective pressures may prove elusive when targeting the microbiome, even if the inhibitors are nonlethal to cultured bacteria in nutrient-rich broths and fail to demonstrate reduction in microbial fitness with prolonged exposures. As the proportions of several taxa reduced by inhibitor exposure were also associated with both TMAO levels and shortened time to arterial occlusion, with chronic inhibitor use, it appears likely that some of the potential efficacy of this family of inhibitors in suppressing TMAO levels also occurs by shifting of microbial composition to one less prone to produce TMA. This effect of the inhibitors appears to be secondary, and it is worth noting that substantial reductions in TMA and TMAO production can be detected rapidly at 1 h post oral gavage of inhibitor concurrently with isotope-labeled choline precursor (Supplementary Fig. 19). It is also noteworthy that many drugs induce shifts in microbial community

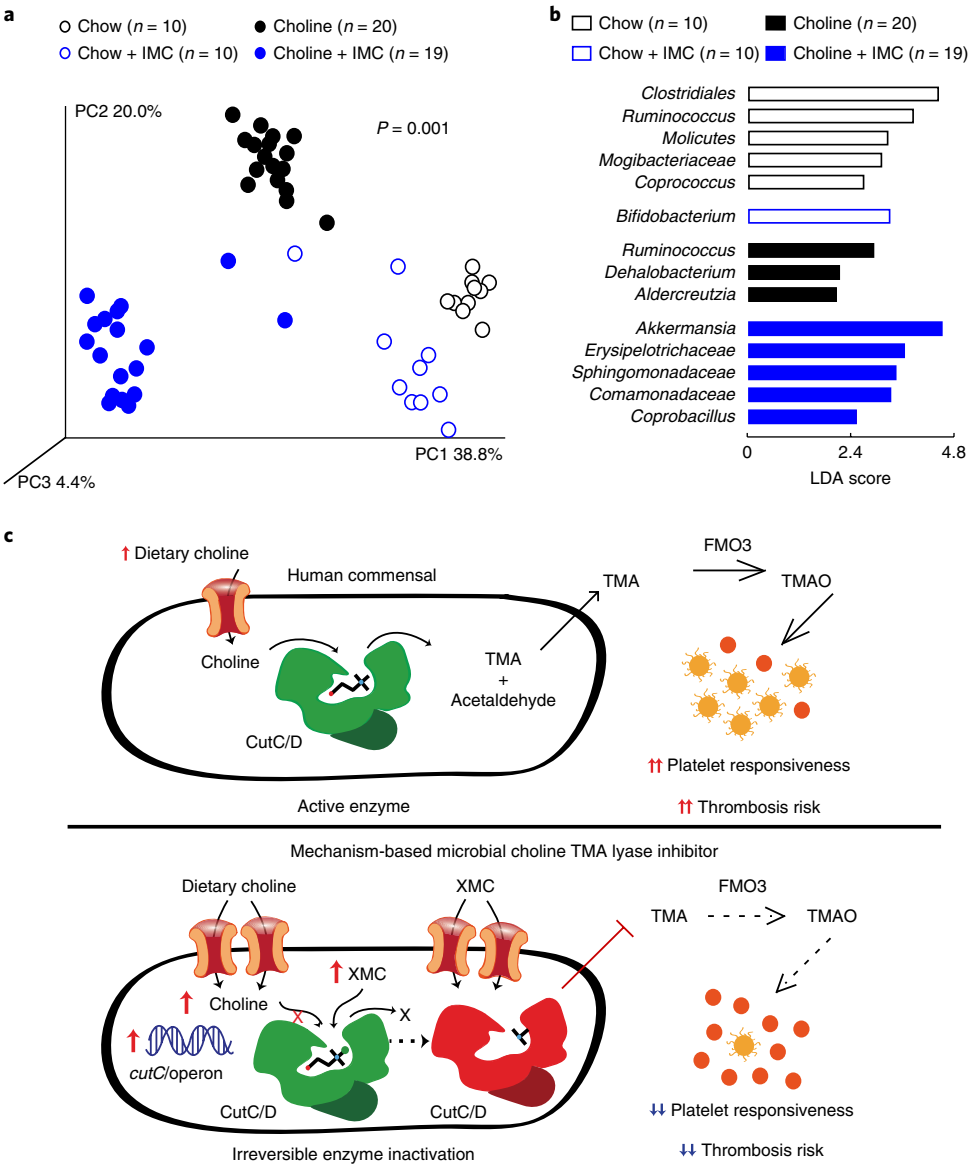

Fig. 5 | A microbial choline TMA lyase inhibitor reverses diet-induced changes in cecal microbial community composition associated with plasma TMAO levels, platelet responsiveness, and in vivo thrombosis potential. a,b, The intestinal microbial community composition of the cecal contents of mice maintained on the indicated diets with or without IMC (0.06% wt/wt) for 2 weeks were assessed by principal coordinate analysis (**a**) or linear discriminant analysis (LDA) effect size (LEfSe) (**b**). **c**, Top, Schematic of the relationship between human gut commensal choline TMA lyase activity, TMA and TMAO generation, and enhanced platelet responsiveness and thrombosis risk in the host. Bottom, Illustration of the impact of halomethylcholine mechanism-based microbial choline TMA lyase inhibitors (XMC) on human commensal TMA generation, host TMAO generation, platelet responsiveness, and thrombosis potential. Upon irreversible enzymatic inhibition of CutC, microbial cytosolic choline increases. Choline is sensed as an abundant nutrient, leading to upregulation of the *cut* gene cluster, including *cutC* and choline active-transporter. Choline and the halomethylcholine inhibitor are actively pumped into the microbe and accumulate. Sequestration of choline in the microbe also depletes the levels of choline available to neighboring microbes, further preventing production of TMA from the gut microbial community and contributing to a reduction in systemic TMA and TMAO levels in the host. The net effect is reduction in platelet aggregation responsiveness to multiple agonists and reduced thrombosis potential in the host.

composition[57,58]. In a recent examination of over 1,000 clinically used drugs and their impact on a broad selection of human gut commensals, nearly a quarter demonstrated antibiotic-like side effects[59]. And in a recent elegant study with metformin, a shift in microbial community structure was suggested to contribute in part to its observed beneficial metabolic effects[60].

The present studies suggest development of poorly absorbed suicide substrate inhibitors of gut microbial catabolic pathways mechanistically linked with disease pathogenesis deserves further investigation as a potentially generalizable approach to achieve therapeutic outcomes in the host. By inhibiting gut microbial production of TMA, we suppressed plasma TMAO levels for prolonged periods with limited systemic exposure of the drugs within the host, reversing choline diet–induced increases in platelet responses to agonists and thrombus formation in vivo. We observed an almost complete reduction in TMA at the site of action in the large intestine with a parallel buildup of inhibitor within the microbe to concentrations 1-million-fold higher than necessary to achieve inhibition within the microbe. A shift in cecal microbial community induced by the inhibitor, when sustained with chronic administration, may contribute to reduction in systemic TMA and TMAO levels in the host. Importantly, no evidence of systemic

toxicity was observed, and our treatment did not adversely affect bleeding potential, a common side effect of traditional antiplatelet therapies. These studies suggest a new potential target for the treatment of subjects at risk for thrombotic complications and cardiovascular disease.

Methods

Methods, including statements of data availability and any associated accession codes and references, are available at https://doi.org/10.1038/s41591-018-0128-1.

Received: 13 October 2017; Accepted: 31 May 2018;
Published online: 06 August 2018

References

1. Kau, A. L., Ahern, P. P., Griffin, N. W., Goodman, A. L. & Gordon, J. I. Human nutrition, the gut microbiome and the immune system. *Nature* **474**, 327–336 (2011).
2. Blaser, M. J. The microbiome revolution. *J. Clin. Invest.* **124**, 4162–4165 (2014).
3. Fischbach, M. A. & Segre, J. A. Signaling in host-associated microbial communities. *Cell* **164**, 1288–1300 (2016).
4. Aron-Wisnewsky, J. & Clément, K. The gut microbiome, diet, and links to cardiometabolic and chronic disorders. *Nat. Rev. Nephrol.* **12**, 169–181 (2016).
5. Schroeder, B. O. & Bäckhed, F. Signals from the gut microbiota to distant organs in physiology and disease. *Nat. Med.* **22**, 1079–1089 (2016).
6. Koopen, A. M., Groen, A. K. & Nieuwdorp, M. Human microbiome as therapeutic intervention target to reduce cardiovascular disease risk. *Curr. Opin. Lipidol.* **27**, 615–622 (2016).
7. Wang, Z. et al. Gut flora metabolism of phosphatidylcholine promotes cardiovascular disease. *Nature* **472**, 57–63 (2011).
8. Tang, W. H. W. et al. Intestinal microbial metabolism of phosphatidylcholine and cardiovascular risk. *N. Engl. J. Med.* **368**, 1575–1584 (2013).
9. Koeth, R. A. et al. Intestinal microbiota metabolism of L-carnitine, a nutrient in red meat, promotes atherosclerosis. *Nat. Med.* **19**, 576–585 (2013).
10. Wang, Z. et al. Prognostic value of choline and betaine depends on intestinal microbiota-generated metabolite trimethylamine-*N*-oxide. *Eur. Heart J.* **35**, 904–910 (2014).
11. Tang, W. H. W. et al. Prognostic value of elevated levels of intestinal microbe-generated metabolite trimethylamine-*N*-oxide in patients with heart failure: refining the gut hypothesis. *J. Am. Coll. Cardiol.* **64**, 1908–1914 (2014).
12. Tang, W. H. W. et al. Gut microbiota–dependent trimethylamine *N*-oxide (TMAO) pathway contributes to both development of renal insufficiency and mortality risk in chronic kidney disease. *Circ. Res.* **116**, 448–455 (2015).
13. Tang, W. H. W. et al. Intestinal microbiota–dependent phosphatidylcholine metabolites, diastolic dysfunction, and adverse clinical outcomes in chronic systolic heart failure. *J. Card. Fail.* **21**, 91–96 (2015).
14. Organ, C. L. et al. Choline diet and its gut microbe–derived metabolite, trimethylamine *N*-oxide, exacerbate pressure overload–induced heart failure. *Circ. Heart Fail.* **9**, e002314 (2016).
15. Zhu, W. et al. Gut microbial metabolite TMAO enhances platelet hyperreactivity and thrombosis risk. *Cell* **165**, 111–124 (2016).
16. Senthong, V. et al. Intestinal microbiota–generated metabolite trimethylamine-*N*-oxide and 5-year mortality risk in stable coronary artery disease: the contributory role of intestinal microbiota in a COURAGE-like patient cohort. *J. Am. Heart Assoc.* **5**, e002816 (2016).
17. Warrier, M. et al. The TMAO-generating enzyme flavin monooxygenase 3 is a central regulator of cholesterol balance. *Cell Rep.* **10**, 326–338 (2015).
18. Seldin, M. M. et al. Trimethylamine *N*-oxide promotes vascular inflammation through signaling of mitogen-activated protein kinase and nuclear factor-κB. *J. Am. Heart Assoc.* **5**, e002767 (2016).
19. Li, T., Chen, Y., Gua, C. & Li, X. Elevated circulating trimethylamine *N*-oxide levels contribute to endothelial dysfunction in aged rats through vascular inflammation and oxidative stress. *Front. Physiol.* **8**, 350 (2017).
20. Yue, C. et al. Trimethylamine *N*-oxide prime NLRP3 inflammasome via inhibiting ATG16L1-induced autophagy in colonic epithelial cells. *Biochem. Biophys. Res. Commun.* **490**, 541–551 (2017).
21. Yano, J. M. et al. Indigenous bacteria from the gut microbiota regulate host serotonin biosynthesis. *Cell* **161**, 264–276 (2015).
22. Fusaro, M. et al. Vitamin K plasma levels determination in human health. *Clin. Chem. Lab. Med* **55**, 789–799 (2017).
23. Jäckel, S. et al. Gut microbiota regulate hepatic von Willebrand factor synthesis and arterial thrombus formation via Toll-like receptor-2. *Blood* **130**, 542–553 (2017).
24. Zhu, W., Wang, Z., Tang, W. H. W. & Hazen, S. L. Gut microbe-generated trimethylamine *N*-oxide from dietary choline is prothrombotic in subjects. *Circulation* **135**, 1671–1673 (2017).
25. Heianza, Y., Ma, W., Manson, J. E., Rexrode, K. M. & Qi, L. Gut microbiota metabolites and risk of major adverse cardiovascular disease events and death: a systematic review and meta-analysis of prospective studies. *J. Am. Heart Assoc.* **6**, e004947 (2017).
26. Schiattarella, G. G. et al. Gut microbe–generated metabolite trimethylamine-*N*-oxide as cardiovascular risk biomarker: a systematic review and dose–response meta-analysis. *Eur. Heart J.* **38**, 2948–2956 (2017).
27. Qi, J. et al. Circulating trimethylamine *N*-oxide and the risk of cardiovascular diseases: a systematic review and meta-analysis of 11 prospective cohort studies. *J. Cell. Mol. Med.* **22**, 185–194 (2018).
28. Brown, J. M. & Hazen, S. L. Targeting of microbe-derived metabolites to improve human health: The next frontier for drug discovery. *J. Biol. Chem.* **292**, 8560–8568 (2017).
29. Dolphin, C. T., Janmohamed, A., Smith, R. L., Shephard, E. A. & Phillips, I. R. Missense mutation in flavin-containing mono-oxygenase 3 gene, FMO3, underlies fish-odour syndrome. *Nat. Genet.* **17**, 491–494 (1997).
30. Bennett, B. J. et al. Trimethylamine-*N*-oxide, a metabolite associated with atherosclerosis, exhibits complex genetic and dietary regulation. *Cell Metab.* **17**, 49–60 (2013).
31. Phillips, G. B. The lipid composition of human bile. *Biochim. Biophys. Acta* **41**, 361–363 (1960).
32. Craciun, S., Marks, J. A. & Balskus, E. P. Characterization of choline trimethylamine-lyase expands the chemistry of glycyl radical enzymes. *ACS Chem. Biol.* **9**, 1408–1413 (2014).
33. Romano, K. A., Vivas, E. I., Amador-Noguez, D. & Rey, F. E. Intestinal microbiota composition modulates choline bioavailability from diet and accumulation of the proatherogenic metabolite trimethylamine-*N*-oxide. *MBio* **6**, e02481 (2015).
34. Martínez-del Campo, A. et al. Characterization and detection of a widely distributed gene cluster that predicts anaerobic choline utilization by human gut bacteria. *MBio* **6**, e00042–15 (2015).
35. Wang, Z. et al. Non-lethal inhibition of gut microbial trimethylamine production for the treatment of atherosclerosis. *Cell* **163**, 1585–1595 (2015).
36. Furie, B. & Furie, B. C. Mechanisms of thrombus formation. *N. Engl. J. Med.* **359**, 938–949 (2008).
37. Bobadilla, R. V. Acute coronary syndrome: focus on antiplatelet therapy. *Crit. Care Nurse* **36**, 15–27 (2016).
38. Levine, G. N. et al. 2016 ACC/AHA guideline focused update on duration of dual antiplatelet therapy in patients with coronary artery disease: a report of the American College of Cardiology/American Heart Association Task Force on Clinical Practice Guidelines. *J. Thorac. Cardiovasc. Surg.* **152**, 1243–1275 (2016).
39. Jennings, L. K. Mechanisms of platelet activation: need for new strategies to protect against platelet-mediated atherothrombosis. *Thromb. Haemost.* **102**, 248–257 (2009).
40. Manchikanti, L. et al. Assessment of bleeding risk of interventional techniques: a best evidence synthesis of practice patterns and perioperative management of anticoagulant and antithrombotic therapy. *Pain. Physician* **16**, SE261–SE318 (2013).
41. Cohen, M. Expanding the recognition and assessment of bleeding events associated with antiplatelet therapy in primary care. *Mayo Clin. Proc.* **84**, 149–160 (2009).
42. Bodea, S., Funk, M. A., Balskus, E. P. & Drennan, C. L. Molecular basis of C–N bond cleavage by the glycyl radical enzyme choline trimethylamine-lyase. *Cell Chem. Biol.* **23**, 1206–1216 (2016).
43. Chen, M. L. et al. Resveratrol attenuates trimethylamine-*N*-oxide (TMAO)-induced atherosclerosis by regulating TMAO synthesis and bile acid metabolism via remodeling of the gut microbiota. *MBio* **7**, e02210–e02215 (2016).
44. Walsh, C. T. Suicide substrates, mechanism-based enzyme inactivators: recent developments. *Annu. Rev. Biochem.* **53**, 493–535 (1984).
45. Hazen, S. L., Zupan, L. A., Weiss, R. H., Getman, D. P. & Gross, R. W. Suicide inhibition of canine myocardial cytosolic calcium-independent phospholipase A2. Mechanism-based discrimination between calcium-dependent and -independent phospholipases A2. *J. Biol. Chem.* **266**, 7227–7232 (1991).
46. Sandhu, S. S. & Chase, T. Jr. Aerobic degradation of choline by *Proteus mirabilis*: enzymatic requirements and pathway. *Can. J. Microbiol.* **32**, 743–750 (1986).
47. Romano, K. A. et al. Metabolic, epigenetic, and transgenerational effects of gut bacterial choline consumption. *Cell Host Microbe* **22**, 279–290.e7 (2017).
48. Nemzek, J. A., Bolgos, G. L., Williams, B. A. & Remick, D. G. Differences in normal values for murine white blood cell counts and other hematological parameters based on sampling site. *Inflamm. Res.* **50**, 523–527 (2001).
49. Koeth, R. A. et al. γ-Butyrobetaine is a proatherogenic intermediate in gut microbial metabolism of l-carnitine to TMAO. *Cell Metab.* **20**, 799–812 (2014).
50. Liu, Y., Jennings, N. L., Dart, A. M. & Du, X.-J. Standardizing a simpler, more sensitive and accurate tail bleeding assay in mice. *World J. Exp. Med.* **2**, 30–36 (2012).
51. Derrien, M., Belzer, C. & de Vos, W. M. *Akkermansia muciniphila* and its role in regulating host functions. *Microb. Pathog.* **106**, 171–181 (2017).

52. Gachet, C. Antiplatelet drugs: which targets for which treatments? *J. Thromb. Haemost.* **13**, S313–S322 (2015).
53. Osbourn, A. E. & Field, B. Operons. *Cell. Mol. Life Sci.* **66**, 3755–3775 (2009).
54. Craciun, S. & Balskus, E. P. Microbial conversion of choline to trimethylamine requires a glycyl radical enzyme. *Proc. Natl Acad. Sci. USA* **109**, 21307–21312 (2012).
55. Berthoumieux, S. et al. Shared control of gene expression in bacteria by transcription factors and global physiology of the cell. *Mol. Syst. Biol.* **9**, 634 (2013).
56. Clarke, D. D. Fluoroacetate and fluorocitrate: mechanism of action. *Neurochem. Res.* **16**, 1055–1058 (1991).
57. Imhann, F. et al. Proton pump inhibitors affect the gut microbiome. *Gut* **65**, 740–748 (2016).
58. Rogers, M. A. M. & Aronoff, D. M. The influence of non-steroidal anti-inflammatory drugs on the gut microbiome. *Clin. Microbiol. Infect.* **22**, 178.e1–178.e9 (2016).
59. Maier, L. et al. Extensive impact of nonantibiotic drugs on human gut bacteria. *Nature* **555**, 623–628 (2018).
60. Wu, H. et al. Metformin alters the gut microbiome of individuals with treatment-naive type 2 diabetes, contributing to the therapeutic effects of the drug. *Nat. Med.* **23**, 850–858 (2017).

Acknowledgements

We appreciate the aid of J. A. Drazba and G. Deshpande of the Lerner Research Institute Imaging Core in studies using the Cellix microfluidic system. This research was supported by grants from the National Institutes of Health (NIH) and the Office of Dietary Supplements (HL103866, HL126827 and DK106000 (to S.L.H.), HL122283 and AA024333 (to J.M.B.), and HL28481 and HL30568 (to A.J.L.)). S.L.H. reports being supported in part by a grant from the Leducq Foundation. V.G. acknowledges a Faculty Research Development Award from Cleveland State University. A.B.R. was supported in part by a grant from the American Heart Association (15POST25750053). W.Z. was supported in part by an AHA Scientist Development Grant and an NIH StrokeNet Clinical Research and Training Grant. S.M.S. was supported in part by training grant T32DK007470 from the National Institute of Diabetes and Digestive and Kidney Disease (NIDDK) of the NIH. Some of the toxicology and safety studies were performed by Pharmaron. Mass spectrometry studies were performed on instrumentation housed in a facility supported in part through a Shimadzu Center of Excellence award. Computational resources were provided by the Extreme Science and Engineering Discovery Environment (National Science Foundation).

Author contributions

A.B.R, J.A.B., and X.G designed, performed, and analyzed data from most of the studies. They also helped write the manuscript with input from all authors. A.G.H., A.D., V.G., A.J.M., and B.S.L aided in chemical synthesis and characterization of all compounds, computational drug design efforts, docking analyses, and quantum mechanical calculations. Z.W. and X.F. helped with design and performance of mass spectrometry analyses. W.Z., N.G., and M.W.R. helped in the design and performance of platelet functional studies, in vivo thrombosis, and other mouse experiments. S.M.S., J.M.L., L.L, W.T.B., and A.J.L. participated in microbe composition analyses and *cut* gene cluster transcription quantification studies. D.B.C., J.M.R., and J.C.G.-G. helped design and perform some of the human commensal and polymicrobial bioreactor studies characterizing inhibitor efficacy. J.A.D. provided overall advice, as well as performing plasmid cloning and construction use in multiple bacterial inhibitor studies. S.R., J.M.B., and J.C.G.-G. provided critical scientific input and discussions. S.L.H conceived, designed, and supervised all studies, and participated in the drafting and editing of the manuscript. All authors contributed to the critical review of the manuscript.

Competing interests

S.L.H., X.G., Z.W., and B.S.L. are named as co-inventors on pending and issued patents held by the Cleveland Clinic relating to cardiovascular diagnostics or therapeutics. S.L.H., Z.W., and B.S.L. report having the right to receive royalty payment for inventions or discoveries related to cardiovascular diagnostics from Cleveland Heart Lab, Inc. and Quest Diagnostics. S.L.H. also reports having been paid as a consultant for P&G and receiving research funds from Astra Zeneca, P&G, Pfizer Inc., and Roche Diagnostics.

Additional information

Supplementary information is available for this paper at https://doi.org/10.1038/s41591-018-0128-1.

Correspondence and requests for materials should be addressed to S.L.H.

Methods

Ethical considerations. All animal model studies were approved by the Institutional Animal Care and Use Committee at the Cleveland Clinic. All study protocols and informed consent for human subjects were approved by the Cleveland Clinic Institutional Review Board. Informed consents were obtained for all subject samples. All studies complied with all relevant animal and human use guidelines and ethical regulations.

In vivo carotid artery thrombosis models. C57BL/6J female mice (6–10 weeks of age) were fed a chemically defined diet comparable to normal chow (0.08% total choline) versus the same chemically defined diet supplemented with 0.5% or 1% wt/wt choline (Envigo TD.140294 and TD.09041, respectively). Half of the mice were treated with TMA lyase inhibitors (DMB, IMC, or FMC) in their diet for more than 1 week. Mice (>12 weeks of age) were anaesthetized (100 mg/kg ketamine and 10 mg/kg xylazine) and subjected to common carotid artery injury by application of 10% $FeCl_3$ for 1 min as previously described[15].

Mouse ex vivo platelet aggregometry studies. C57BL/6J female mice (6–10 weeks of age) were fed a chemically defined diet comparable to normal chow (0.08% total choline) versus the same chemically defined diet supplemented with either 0.5% or 1% wt/wt choline (Envigo TD.140294 and TD.09041, respectively as indicated). Half of the mice were treated with TMA lyase inhibitors (DMB, IMC, or FMC) in their diet for more than 1 week. Mice (>12 weeks of age) were anesthetized with (100 mg/kg ketamine and 10 mg/kg xylazine), and blood samples were collected and analyzed for ex vivo aggregation response as previously described[15].

Recombinant TMA lyase inhibition assays. Enzymatic assays were conducted to measure the conversion of choline to TMA using an isotope-labeled version of choline (d_9[trimethyl]-choline). Clarified lysate was diluted to 5 mg/mL in lysis buffer, and the necessary cofactors were added (1 mM S-adenosyl methionine (SAM), 10 mM NaDT, and 2 mM NADH). Individual 400-µL aliquots were added to 13×100 mm threaded glass tubes with gas-tight mininert caps. Potential inhibitor compounds were serially diluted (tenfold) and added to the reaction mixtures. Each inhibitor concentration was done in triplicate. The mixture was then allowed to incubate for 15 min before the addition of substrate (300 µM final) to initiate the reaction, which was carried out for 2 h at room temperature in the dark. Whole-cell assays were conducted similarly at 37 °C. The relevant cell cultures were diluted 1:100 in lysogeny broth (LB) medium and shaken at 37 °C until an optical density at 600 nm (OD_{600}) = 0.5 was reached. At this point, the cells were aliquoted (400 µL) in 13×100 mm threaded glass tubes with gas-tight mininert caps. Without the need for cofactors, the reaction was initiated with the addition of d_9-labeled substrate after a period of incubation with potential inhibitor compounds. Whole-cell reactions were carried out at 37 °C for 2 h. For each experiment, 'no addition' (vehicle) controls were used to calculate 100% relative activity. Reactions were quenched 15 min after substrate addition (during the initial, linear kinetic phase) for the analysis of time-dependence and Michaelis–Menten kinetics.

The reversibility of inhibitors was tested by overnight dialysis. Crude lysate was prepared, as previously described (with or without addition of 10 µM inhibitor), before addition to 3,500 MWCO Slide-A-Lyzer Mini Dialysis Units (Pierce, Rockford, IL) in triplicate. Each unit was floated on ~500 mL of lysis buffer for 2 h with gentle stirring at 4 °C. The buffer was then changed before stirring continued overnight. Reaction samples were also prepared without dialysis and left overnight at 4 °C as a control. Reactions were initiated the next day with the addition of substrate and carried out as previously described above.

The reactions were quenched with the addition of 200 µL of 1 M NaOH, and 8 µL of 25 µM [$^{13}C_3{}^{15}N_1$]TMA (Sigma Chemicals, St. Louis, MO) was added as the internal standard before placement on ice. After 15 min, 1.6 mL lysis buffer, 2 mL hexane, and 1 mL butanol were added to each reaction mixture. The tubes were then vortexed for 1 min and centrifuged at 2,500 *g* for 10 min. The top, organic layer was then transferred to a 12×75 mm PTFE capped threaded glass tube, acidified with the addition of 200 µL of 0.2 N formic acid, vortexed, and the organic and aqueous layers were separated by centrifugation. After centrifugation, an aliquot of formic acid containing the d_9-TMA product was transferred to a mass spectrometry vial containing a plastic insert for quantification by stable isotope dilution liquid chromatography with on-line tandem mass spectrometry (LC–MS/MS) analysis.

All data analyses were performed in GraphPad Prism. For IC_{50} calculations, the data were fit to a nonlinear regression equation (normalized response, variable slope). For time-dependence, the data were fit to the dissociation (one phase exponential decay) equation. For Michaelis–Menten, the curves were fit (along with calculations of K_M and V_{max}) by nonlinear regression ('Michaelis–Menten').

Quantification of d_9-TMA. Samples were injected onto a reverse-phase C18 HPLC column and resolved with a linear gradient between 0.2% formic acid in water and 0.2% formic acid in an acetonitrile–methanol mixture (95:5 vol/vol). The effluent was analyzed by an AB Sciex 5500 QTRAP mass spectrometer using electrospray ionization in the positive-ion mode. TMA was quantified by measuring the peak area ratio of the precursor to product ion transition of d_9-TMA (m/z 69 →49) to the internal standard [$^{13}C_3{}^{15}N_1$]TMA (m/z 64 → 47).

Human fecal polymicrobial assay. Human fecal samples were collected from healthy volunteers with no known chronic illnesses, blood-borne diseases, or active infections. The volunteers had not received antibiotics within 2 months of donation and provided written informed consent. Samples were diluted to make a 20% (wt/vol) fecal slurry by resuspension of the feces in a medium containing 3% (wt/vol) tryptic soy broth, 1% (wt/vol) trehalose, pH 7.3. The fecal slurry was homogenized and filtered by hand using a stomacher bag with an integrated 170-µm membrane. DMSO (5% (wt/vol) was added to the filtered slurry, and aliquots were stored in cryogenic vials at −80 °C until use. Frozen fecal slurries were diluted to 0.2% (wt/vol) with M9 medium (Na_2HPO_4 (6 g/L), KH_2PO_4 (3 g/L), NaCl (0.5 g/L) with addition of 0.1 mM $CaCl_2$ and 1 mM $MgSO_4$) and dispensed (1 mL) into deep-well 96-well plates. Diluted fecal slurries containing 50 µM d_9-choline chloride and halomethylcholine and halomethylbetaine compounds in doses ranging from 3.81 nM to 250 µM were sealed and incubated at 37 °C with shaking. After 20 h, an aliquot of the fecal polymicrobial community was analyzed for viability using Prestoblue cell viability reagent following the manufacturer's instructions (Thermo Fisher Scientific). The reaction plates were subsequently centrifuged (4,000 *g* at 4 °C for 12 min) to pellet fecal material, and 150-µL aliquots were transferred and quenched with addition of formic acid to 1% (vol/vol). All fecal processing and polymicrobial assay steps were performed in an anaerobic environment. The products were determined by LC–MS/MS, and IC_{50} values were calculated as described previously for detection and analysis of TMA and d_9-TMA in wild-type *P. mirabilis* cell lysates.

Quantitation of in vivo TMAO, TMA, choline, betaine, IMC, IMB, FMC, and FMB. LC–MS/MS was used for quantification of levels of TMAO, TMA, choline, and betaine in plasma, urine, fecal, and tissue as previously described[7,35,61]. Their isotope (d_9)-labeled analogs were used as internal standards. For IMC quantification, d_2-IMC was used as an internal standard, and for FMC, d_9-choline was used as an internal standard. For IMB and FMB quantification, d_9-betaine was used as an internal standard. LC–MS/MS analyses were performed on a Shimadzu 8050 triple quadrupole mass spectrometer. Although not observed in vivo, levels of I-TMA, iodo-trimethylamine-*N*-oxide (I-TMAO), fluoro-trimethylamine (F-TMA), and fluoro-trimethylamine-*N*-oxide (F-TMAO) were monitored at predicted transitions using multiple reaction monitoring of precursor and characteristic from CID spectra of synthetic standards product ions: m/z 186.1 → 44.2 for I-TMA; m/z 202 → 184 for I-TMAO; m/z 78.1→ 44.2 for F-TMA; m/z 94 → 76 for F-TMAO. Levels of TMAO, d_9-TMAO, TMA, d_9-TMA, choline, d_9-choline, betaine, d_9-betaine, IMC, d_2-IMC, IMB, FMC, and FMB were monitored using multiple reaction monitoring of precursor and characteristic product ions: m/z 76.0 → 58.1 for TMAO; m/z 85.0 → 66.25 for d_9-TMAO; m/z 60.2 → 44.2 for TMA; m/z 69.0 → 49.1 for d_9-TMA; m/z 104.0 → 60.15 for choline; m/z 113.1 → 69.2 for d_9-choline; m/z 118.0 → 58.1 for betaine; m/z 127.0 → 66.2 for d_9-betaine; m/z 230.0 → 58.05 for IMC; m/z 232.0 → 60.1 for d_2-IMC; m/z 244.0 → 58.1 for IMB; m/z 122.1 → 58.05 for FMC; m/z 136 → 58.1 for FMB.

Effects on plasma TMAO levels. For our 'q24h post-gavage' model, C57BL/6J female mice (12 weeks of age; obtained from Jackson Laboratory, no. 0664) were placed on 1% wt/wt choline diet (Teklad, no. TD.09041) and given either vehicle, IMC, or FMC at concentrations ranging from 1.8 to 310 mg/kg once daily via gavage. Blood was collected 24 h postgavage at the indicated days. For our 'd_9-choline challenge' model, C57BL/6J female mice (18–20 g average body weight) fed normal chow were fasted for 1 h. At this point, 2 mg d_9-choline in 0.2 mL of sterile water was given via oral gavage in combination with either vehicle, IMC, or FMC at concentrations ranging from 0.0001 to 100 mg/kg. The dietary fast was continued for 1 h postgavage. Blood was collected 3 h postgavage. For blood collection, mice were restrained in a rodent restraint tube. A 26-G needle was used to lance the saphenous vein. Blood was collected into a heparin-treated capillary tube and was spun in a capillary centrifuge (12,000 r.p.m., 5 min, 4 °C) to separate plasma. Samples were acidified (60 mM HCl final) for analysis of TMA levels before flash freezing and storage in gas-tight vials at −80 °C.

In vivo toxicity studies. C57BL/6J female mice (8–12 weeks of age, obtained from Jackson Laboratory, no. 664) were placed on 1% wt/wt choline diet (Teklad, no. TD.09041) and given inhibitor or vehicle (water) once daily via gavage. Blood and urine were collected at the indicated days (4, 11, and 14 days after diet start). On day 14, mice were humanely euthanized by anesthesia overdose (>300 mg/kg ketamine + 30 mg/kg xylazine), and blood was collected for analysis of physiologic markers of toxicity. EDTA-treated whole blood from mice treated for 14 d was run on a Siemens Advia 120 Hematology Analyzer for CBC with differential. Plasma was analyzed for liver (ALT, AST) and kidney function (BUN) using a Roche Cobas C 311 analyzer, and CBC with differential was determined using a Bayer Advia hematology analyzer.

Pharmacokinetics. C57BL/6J female mice (13 weeks of age, obtained from Jackson Laboratory, no. 664) were placed on 1% wt/wt choline-supplemented diet (Teklad, no. TD.09041) for at least 1 week before the start of the experiment. Mice were given a single oral dose of inhibitor via gastric gavage at 100 mg/kg. Whole-blood samples were collected at the indicated time points postgavage and were

treated with EDTA or heparin. Samples were either centrifuged at 4,000 r.p.m. at 4 °C /for 20 min or collected into a heparin-treated capillary tube and was spun in a capillary centrifuge (12,000 rpm, 5 min, 4 °C) to separate and collect plasma before 1:4 dilution in cold methanol (containing internal standards). Urine samples were collected in 1.5-mL Eppendorf tubes. Samples were diluted 1:32 in sterile water and then diluted 1:4 in cold methanol (containing internal standards). Fecal samples were collected, vacuum-dried, and weighed. Samples were homogenized in 2-mL cryovials with the addition of 1 mL sterile water and ~200 µL acid-washed glass beads (< 106 µm). Samples were then lysed using a TissueLyser II (Qiagen) at 30 m/s for 12 min before centrifugation (12,000 r.p.m., 4 °C, 30 min). Aliquots of the supernatants were diluted 1:4 in cold methanol (containing internal standards). LC–MS/MS was used to measure levels of plasma, urine, and fecal metabolites.

Intestinal luminal content analyses. C57BL/6 J female mice (13 weeks of age; obtained from Jackson Laboratory, no. 664) were placed on 1% wt/wt choline diet (Teklad, no. TD. 09041) for 3 weeks before the start of the experiment. Mice were given a single dose of vehicle or 100 mg/kg of compound via gavage. Four hours postgavage, animals were humanely euthanized by anesthesia overdose (>300 mg/kg ketamine + 30 mg/kg xylazine), and the small intestine, cecum, and colon were collected. Starting at the pyloric sphincter, the small intestine was segmented into three equal segments (duodenum, jejunum, ileum), and 1 mL of buffer (200 mM HEPES, 50 mM NaCl, 10 mM $MgCl_2$, pH 8.0) was used to flush lumen. Cecum and colon were separated and flushed, and content was expelled by force. Precise concentrations of metabolites was measured by calculating a dilution factor based on the mass of buffer (assuming density = 1 mg/mL) and the change in mass before and after flushing of luminal contents and removal of intestinal tissue. Intestinal contents were transferred to a 2-mL cryovial with the addition of ~200 µL acid-washed glass beads (< 106 µm). Samples were then lysed using a TissueLyser II (Qiagen) at 30 m/s for 12 min before centrifugation (12,000 r.p.m., 4 °C, 30 min). Aliquots of the supernatants were diluted 1:4 in cold methanol (containing internal standards). Levels of metabolites were quantified by LC–MS/MS as described above.

Quantification of *cutC* RNA via qPCR. Real-time qPCR was used to amplify *cutC* using degenerate primers via a method adapted from genomic analysis of *cutC* abundance. C57BL/6 J female mice (10–13 weeks of age) were started on diets of either minimal choline or choline-supplemented (1% wt/wt) with or without the addition of FMC (0.006%) or IMC (0.06%) for 2 weeks. Mice were humanely euthanized (300 mg/kg ketamine and 30 mg/kg xylazine). Whole ceca were harvested and flash frozen in liquid nitrogen and stored at –80 °C. The cecal contents were excised on dry ice to minimize thawing of the sample. RNA isolation was performed using the PowerMicrobiome RNA Isolation Kit (Qiagen). Frozen cecal contents (~10 mg) were added to the provided tubes. 1.5 mL of chilled QIAzol (Qiagen) was added to each sample. Samples were immediately homogenized on the TissueLyzer LT (Qiagen) at 50 m/s. Three rounds of 2-min lysing periods were each separated by 1 min on ice to minimize RNA degradation. Chloroform (0.3 mL) was added to each sample and vortexed, and then samples were centrifuged at 12,000*g* and 4 °C for 10 min. The aqueous phase was isolated and used to carry out the remainder of the RNA isolation as described in the PowerMicrobiome RNA Isolation Kit instruction manual. RNA concentration was quantified using a Nanodrop 1000 spectrophotometer (Thermo Fisher). RNA (400 ng) was converted to cDNA using the High-Capacity cDNA Reverse Transcriptase Kit with random primers (Applied Biosystems). Transcript abundance of *cutC* was normalized to universal 16 S ribosomal RNA abundance. Degenerate primer sequences used were[62]: *cutC* (forward) 5′- AGRGTTHGATYMTGGCTCAG-3′ and *cutC* (reverse) 5′-TGCTGCCTCCCGTAGGAGT-3′, and 16 S (forward) 5′- TTYGCIGGITAYCARCCNTT and 16 S (reverse) 5′ -TGNGGYTCIACRCAICCCAT-3′. Reactions were run in triplicate using KAPA SYBR FAST qPCR Master Mix (Roche) with 8 ng of cDNA per reaction and 1.5 µM primer concentration. Quantification was performed on the LightCycler 480 (Roche) with an initial 95 °C step for 5 min, followed by 45 cycles of denaturation at 95 °C for 45 s, annealing at 57 °C for 45 s, and an extension at 72 °C for 45 s. Following amplification, a melting point analysis was performed using the following protocol: 95 °C for 5 s, followed by 65 °C for 60 s, and a continuous reading step of seven acquisitions per second between 65 °C and 97 °C. All melting curves were analyzed to ensure each sample had a consistent melting point. Results are expressed as averages of three independent reactions.

Bleeding time analyses. C57BL/6 J female mice (Jackson, no. 664) 8–12 weeks of age were placed on diets ± 1% wt/wt choline (Envigo, TD. 09041; TD 130104) and ± 0.06% IMC or 0.006% FMC for 1 week. Mice were anesthetized (100 mg/kg ketamine + 10 mg/kg xylazine) and maintained on a warming pad to maintain body temperature. A consistent injury was made 3 mm from the tip of the tail. The tail was immersed in 15 mL of 37 °C saline, and the cumulative bleeding time was recorded during a 10-min period. Body weights were recorded before and after bleeding (including the excised tail) to quantify blood loss. Hemoglobin content was measured by spectrophotometry. Red blood cells were isolated from the tail blood–containing saline samples by centrifuging (4,000 r.p.m., 5 min) and removing the supernatant. Pelleted cells were then lysed by hypotonic lysis. Cells were initially resuspended in 900 µL H_2O. After 17 s, 100 µL of 10 × PBS was added and inverted to mix. The solution was then centrifuged at 10,000 r.p.m. for 5 min. The supernatant was saved, and the optical density at 550 nm (OD_{550}) was measured.

Statistical analysis. Unless otherwise indicated, a one- or two-tailed Student's *t*-test or a Wilcoxon nonparametric test was used to compare group means as deemed appropriate. ANOVA _(if normally distributed) or Kruskal–Wallis test (if not normally distributed) was used for multiple-group comparisons of continuous variables, and a Chi-square test was used for categorical variables. A robust Hotelling T2 test was used to examine the difference in the proportion of specific bacterial genera along with TMAO levels or occlusion times between the different dietary and treatment groups. The indicated number of biological replicates were used in all experiments. Results from all animals in a given experiment were included in the analyses. Investigators performing quantitative analyses of endpoints (for example, plasma, urine, or fecal metabolite levels) were blinded to group allocation, and samples were labeled by code only. Investigators were not blinded to mouse group allocation during the performance of animal husbandry requirements for experiments. Unless otherwise noted, most data were analyzed using R software version 2.15 and Prism (GraphPad Software).

Reporting Summary. Further information on experimental design is available in the Nature Research Reporting Summary linked to this article.

Data availability. Data are available from the corresponding author upon reasonable request. The 16 s sequencing datasets generated and analyzed during the current study are available in the NCBI Sequence Read Archive (PRJNA471699).

References

61. Wang, Z. et al. Measurement of trimethylamine-*N*-oxide by stable isotope dilution liquid chromatography tandem mass spectrometry. *Anal. Biochem.* **455**, 35–40 (2014).
62. Rath, S., Heidrich, B., Pieper, D. H. & Vital, M. Uncovering the trimethylamine-producing bacteria of the human gut microbiota. *Microbiome* **5**, 54 (2017).

nature research

Corresponding author(s): Dr. Stanley L. Hazen

☐ Initial submission ☐ Revised version ☒ Final submission

Life Sciences Reporting Summary

Nature Research wishes to improve the reproducibility of the work that we publish. This form is intended for publication with all accepted life science papers and provides structure for consistency and transparency in reporting. Every life science submission will use this form; some list items might not apply to an individual manuscript, but all fields must be completed for clarity.

For further information on the points included in this form, see Reporting Life Sciences Research. For further information on Nature Research policies, including our data availability policy, see Authors & Referees and the Editorial Policy Checklist.

Experimental design

1. Sample size

Describe how sample size was determined.

All experiments were performed at least in triplicate or where otherwise noted, with a larger sample size. Power calculations for in vivo thrombosis studies suggested a group size of at least 5. Results shown often reflect data summed from multiple experiments with cumulatively larger sample sizes.

2. Data exclusions

Describe any data exclusions.

There were no data exclusions

3. Replication

Describe whether the experimental findings were reliably reproduced.

Replicate experiments were performed for all studies as noted in figure legends, methods, and Source Data. Experimental findings were reliably reproduced.

4. Randomization

Describe how samples/organisms/participants were allocated into experimental groups.

Mice in all studies were randomized to their particular groups at time of allocation to experimental groups.

5. Blinding

Describe whether the investigators were blinded to group allocation during data collection and/or analysis.

Investigators performing quantitative analyses of endpoints (e.g., plasma, urine, or fecal metabolite levels and time to vessel occlusion in in vivo thrombosis assays) were blinded to group allocation with samples labeled by code only. Investigators were not blinded to mouse group allocation during the performance of animal husbandry requirements for experiments.

Note: all studies involving animals and/or human research participants must disclose whether blinding and randomization were used.

6. Statistical parameters

For all figures and tables that use statistical methods, confirm that the following items are present in relevant figure legends (or in the Methods section if additional space is needed).

n/a	Confirmed
☐	☒ The exact sample size (*n*) for each experimental group/condition, given as a discrete number and unit of measurement (animals, litters, cultures, etc.)
☐	☒ A description of how samples were collected, noting whether measurements were taken from distinct samples or whether the same sample was measured repeatedly
☐	☒ A statement indicating how many times each experiment was replicated
☐	☒ The statistical test(s) used and whether they are one- or two-sided (note: only common tests should be described solely by name; more complex techniques should be described in the Methods section)
☐	☒ A description of any assumptions or corrections, such as an adjustment for multiple comparisons
☐	☒ The test results (e.g. *P* values) given as exact values whenever possible and with confidence intervals noted
☐	☒ A clear description of statistics including central tendency (e.g. median, mean) and variation (e.g. standard deviation, interquartile range)
☐	☒ Clearly defined error bars

See the web collection on statistics for biologists for further resources and guidance.

Software

Policy information about availability of computer code

7. Software

Describe the software used to analyze the data in this study.	Most data was analyzed using R software version 2.15 and Prism 5 (Graphpad Software). 16S microbial data were analyzed using QIIME version 1.9, SUMACLAST version 1.0.00 and PYNAST version 1.2.2 For docking studies, we used Autodock Vina program (version 1) which is a parallel version of Autodock 4 program. To prepare the enzyme and the ligand for docking, we used MGLTools (version 1.5.7rc1) a graphic interface for Autodock program. We built structures for inhibitors (PDB files and Gamess input files) with the Avogadro program (version 1.2.0). Quantum mechanical calculations were performed with the program Gamess US (MacOSX binary "gamess.18Aug2016R1.x"). We specified the level of QM calculation used (HF/6-31G(d)). Enzymatic fecal polymicrobial data was analyzed by Dotmatics Studies Assay data management and analysis software version 5.1.1. A compensation matrix was applied to the data in the Apogee histogram software. Analysis of prothrombotic markers was done in FlowJo 10.4.

For manuscripts utilizing custom algorithms or software that are central to the paper but not yet described in the published literature, software must be made available to editors and reviewers upon request. We strongly encourage code deposition in a community repository (e.g. GitHub). *Nature Methods* guidance for providing algorithms and software for publication provides further information on this topic.

Materials and reagents

Policy information about availability of materials

8. Materials availability

Indicate whether there are restrictions on availability of unique materials or if these materials are only available for distribution by a for-profit company.	All materials are available from the indicated commercial sources or upon request to the corresponding author

9. Antibodies

Describe the antibodies used and how they were validated for use in the system under study (i.e. assay and species).	All assays included appropriate positive and negative controls as indicated, for assay validation. If applicable, the assays were designed per the manufacturer's instructions. Mouse plasma vWF levels were assessed by using Abcam's (cat# ab208980) vWF A2 (von Willebrand factor A2) in vitro SimpleStep ELISA (Enzyme-Linked Immunosorbent Assay) kit using the manufacturer's instructions. Lot No. GR3197038-1 Annexin V kit: lot no. 7312712: As per manufacturer's instruction 5 ul per test (1:20 dilution not 1:50 as supplementary figure 1 data legend (BD Pharmingen, cat# 556547). FITC-conjugated rat-anti-mouse CD41 (clone MWreg30, BD Biosciences) cat. No. 553848 : citation: https://onlinelibrary.wiley.com/doi/pdf/10.1111j.1538-7836.2008.03188.x For immunoaffinity staining p-selectin analysis, samples were incubated with FITC-CD62p (BD Pharmingen, cat# 561923) at 40ug/ml. http://www.bloodjournal.org/content/122/8/1478/ For Microparticles: Following dilutions were made to titrate abs 1/100, 2/100, 4/100, 8/100 and 16/100 for both abs and based on the titration data on microparticles 8ul was used for Annexin V staining and 5 ul for cd41 staining. PE-CD41 (BD Pharmingen, cat# 558040) and FITC-annexin V (BD Pharmingen, cat# 556547)

10. Eukaryotic cell lines

a. State the source of each eukaryotic cell line used.

HK-2 cells (human papillomavirus 16 (HPV-16) transformed, ATCC® CRL-2190™) and HepG2 (human liver hepatocellular carcinoma cell line, ATCC HB-8065™) were purchased from ATCC.

hERG-T-REXTM 293 cells were initially purchased from Invitrogen (Cat No. K1236) and have been maintaining in Pharmaron since then.

b. Describe the method of cell line authentication used.

We identified the authentication of the HK-2 and HepG2 cell lines by the cellular morphology under microscope.

For hERG cells, as the expression of hERG channel requires the extra addition of doxycycline (or tetracycline), the authentication of cells was established on monitoring the induced transmembrane electrical currents under voltage-clamp configuration.

c. Report whether the cell lines were tested for mycoplasma contamination.

Neither of the HK-2 and HepG2 cell lines were listed in the ICLAC database of commonly misidentified cell lines. We have tested the mycoplasma contamination of the cell lines in some early passages and no mycoplasma contamination was detected.

The routine mycoplasma test for hERG-T-REXTM 293 cells is carried out regularly and no contamination was found ever since.

d. If any of the cell lines used are listed in the database of commonly misidentified cell lines maintained by ICLAC, provide a scientific rationale for their use.

None of the cell lines were listed in the ICLAC database of commonly misidentified cell lines

Animals and human research participants

Policy information about studies involving animals; when reporting animal research, follow the ARRIVE guidelines

11. Description of research animals

Provide details on animals and/or animal-derived materials used in the study.

We used female, wild-type C57BL/6J mice, between 6 to 12 weeks old

Policy information about studies involving human research participants

12. Description of human research participants

Describe the covariate-relevant population characteristics of the human research participants.

Human fecal samples were collected from healthy volunteers with no known chronic illnesses, blood borne diseases or active infections. The volunteers had not received antibiotics within two months of donation and provided written informed consent.

Human blood samples for direct inhibitor addition experiments were collected according to protocol and with informed consent. No patient information was collected.